Universidade de São Paulo
Instituto de Astronomia, Geofísica e Ciências Atmosféricas
Departamento de Astronomia

Aura de las Estrellas Ramírez Arévalo

The Red Supergiants in the Supermassive Stellar Cluster Westerlund 1 (As Supergigantes Vermelhas no Aglomerado Estelar Supermassivo Westerlund 1)

São Paulo

2018

Aura de las Estrellas Ramírez Arévalo

The Red Supergiants in the Supermassive Stellar Cluster Westerlund 1 (As Supergigantes Vermelhas no Aglomerado Estelar Supermassivo Westerlund 1)

Dissertação apresentada ao Departamento de Astronomia do Instituto de Astronomia, Geofísica e Ciências Atmosféricas da Universidade de São Paulo como requisito parcial para a obtenção do título de Mestre em Ciências.

Área de Concentração: Astronomia
Orientador: Prof. Dr. Augusto Damineli Neto

Versão Corrigida. O original encontra-se disponível na Unidade.

São Paulo

2018

To my parents, Eustorgio and Esmeralda, to whom I owe everything.

Acknowledgements

This dissertation was possible thanks to the support of many people, to whom I owe not only this manuscript and the work behind it, but many years of personal and professional growth.

In the first place I thank my parents, Eustorgio and Esmeralda, for all the unconditional love and the sacrifices they have made to make me the woman I am today, for never leaving me alone no matter how far we are, and for all the support they have given me throughout the years, that has allowed me to fulfill my dreams. This accomplishment is theirs. *Papá y mamá, este logro es de ustedes.*

I thank Alex, my companion during this phase, for his love, patience and priceless support especially in those difficult times, when he would cheer me up.

Thanks to my dear friends: Diego R., who welcomed me when I came to Brazil; Andrés and Tatiana, the first friends I made here; Caori, who is always willing to give the best advice; Estefanía, Lina, July, Alejandro, Luis, Wilmar, Diego C., Misael and Rosario, my old and cherished friends who happen to be always there when I'm bored, despite the distance and different time zones.

Thanks to my adviser Professor Augusto Damineli for his guidance and patience throughout this process. His knowledge, experience and feedback have been invaluable to me, as an aspiring astronomer. Thanks to Professor Marcos Diaz, for his comments and suggestions on my semi-annual reports, and thanks to all my teachers at IAG, who have made a priceless contribution both to this work and my professional development. A special place is for Professor Giovanni Pinzón, who introduced me to astrophysics, back in Colombia at the UNAL.

Thanks to my colleagues from the High Mass Stars group: Marcelo, Felipe and Leonardo

for always being willing to help. And thanks to Marcelo and Daiane also for the coffee and fun conversations.

This work would not have been possible without financial support from CAPES through the PROEX program, under process number 1578652. Also, observations were carried out at *Observatório do Pico dos Dias*, operated by the *Laboratório Nacional de Astrofísica* (LNA), and the Southern Astrophysical Research Telescope (SOAR), operated by a partnership between CNPq (Brazil), the U.S. National Optical Astronomy Observatory (NOAO), the University of North Carolina (UNC) and Michigan State University (MSU).

Lastly, I want to thank Brazil, the University of São Paulo and IAG for taking me in during these past two and a half years and for giving me the oportunity to grow in so many ways.

This dissertation was writen in LaTeX with the class IAGTESE, for theses and dissertations from IAG.

"I wonder," he said, "whether the stars are set alight in heaven so that one day each one of us may find his own again."

Antoine de Saint-Exupéry, *The Little Prince*

Resumo

O objetivo desta dissertação é estudar as estrelas Supergigantes Vermelhas (RSGs) no aglomerado jovem supermassivo Westerlund 1 através de uma análise fotométrica e espectral. Devido às suas características, Westerlund 1 é um dos aglomerados jovens mais interessantes da Via Láctea e tem uma população importante de estrelas massivas, com quatro RSGs entre elas. Isso representa uma oportunidade rara para estudar este tipo de estrelas em um aglomerado com a distância e avermelhamento bem conhecidos. Além de contribuir para o conhecimento geral sobre RSGs, cujos parâmetros são pouco conhecidos devido à sua escassez, uma análise dessas quatro estrelas contribuirá para resolver o enigma da história da formação de Westerlund 1.

Para a análise apresentada aqui, foram utilizados dados fotométricos das quatro RSGs em Westerlund 1, juntamente com espectros no infravermelho próximo cobrindo a região de $\sim$ 8400 Å a $\sim$ 8900 Å, obtidos em duas épocas diferentes com o telescópio de 1,60 m do *Observatório do Pico dos Dias* (OPD) e o *Southern Astrophysical Research Telescope* (SOAR). Magnitudes obtidas com a fotometria nos filtros JHK foram usadas para calcular temperaturas efetivas e correções bolométricas na banda K através de diferentes métodos envolvendo os índices de cor $(V-K)_0$ e $(J-K)_0$, a fim de determinar as luminosidades e localizar as quatro RSGs em um diagrama de Hertzsprung-Russell (HRD).

Uma análise espectral foi realizada com o objetivo de estimar os tipos espectrais e os mesmos parâmetros estelares calculados com a fotometria. Primeiramente, uma comparação visual da profundidade e força das principais características espectrais (as bandas moleculares de TiO e VO e as linhas de CaT e Fe I) foi realizada para classificar as estrelas por tipo espectral. Para este propósito, os espectros das quatro RSGs no aglomerado foram comparados com um grupo de espectros de estrelas de referência bem estudadas,

alguns delas também RSGs. Depois, dada a sua forte dependência com a T_{eff}, as larguras equivalentes (EWs) das linhas de Fe I foram medidas em todos os espectros disponíveis. Comparando as EWs medidas nos espectros das quatro RSGs e nos das estrelas de referência, as T_{eff} das estrelas de referência mais similares foram atribuídas às RSGs do aglomerado. Com as T_{eff} obtidas através da análise espectral, novos pontos foram adicionados ao HRD inicial.

O objetivo final do presente trabalho foi estimar as massas iniciais e as idades das RSGs em Westerlund 1. Isto foi realizado através da sobreposição no HRD de caminhos evolutivos e de isócronas. Massas e idades foram determinadas para os casos com e sem rotação, obtendo-se uma média de idade para as RSGs de 8 milhões de anos, duplicando assim a idade do aglomerado ao que as RSGs pertencem, e que foi medida através de estrelas de pré-sequência principal (PMS).

Na parte final, é apresentada uma breve discussão sobre a discrepância da idade de Westerlund 1 medida com as isócronas da PMS e a idade das RSGs, bem como as incertezas que isso suscita em relação à história da formação do aglomerado.

Abstract

The purpose of this dissertation is to study the Red Supergiant stars (RSGs) in the supermassive young cluster Westerlund 1 through a photometric and spectral analysis. Due to its characteristics, Westerlund 1 is one of the most interesting young massive clusters in the Milky Way and has an impressive population of massive stars, with four RSGs among them. This represents a rare oportunity to study this type of stars in a cluster with well known distance and reddening. Apart from contributing to the general knowledge about RSGs, which parameters are poorly known due to their scarcity, an analysis of these four stars will contribute to solve the puzzle of the formation history of Westerlund 1.

For the analysis presented here, photometric data of the four RSGs in Westerlund 1 were used, along with near infrared spectra covering the region from ~ 8400 Å to ~ 8900 Å, obtained at two different epochs with the 1.60 m telescope at *Observatório do Pico dos Dias* (OPD) and the *Southern Astrophysical Research Telescope* (SOAR). Magnitudes obtained with JHK band photometry were used to calculate effective temperatures and bolometric corrections at the K band through different methods involving the color indices $(V-K)_0$ and $(J-K)_0$, in order to determine the luminosities and locate the four RSGs in a Hertzsprung-Russell diagram (HRD).

A spectral analysis was performed with the aim of estimating spectral types and the same stellar parameters calculated with the photomety. First, a visual comparison of the depth and strength of the main spectral features (TiO and VO bandheads, and CaT and Fe I lines) was carried out to classify the stars by spectral type. For this purpose, spectra of the four RSGs in the cluster were compared to a group of spectra from well studied reference stars, some of them also RSGs. Then, given their strong dependence on T_{eff}, equivalent widths (EWs) of Fe I lines were measured in all the spectra available. By

comparing the EWs measured on spectra of the four RSGs and the reference stars, the T_{eff}'s of the most similar reference stars were assigned to the RSGs in the cluster. With the T_{eff}'s obtained through the spectral analysis, new points were added to the initial HRD.

The final objective of the present work was to estimate the initial masses and ages of the RSGs in Westerlund 1. This was accomplished by superimposing up to date evolutionary tracks and isochrones to the HRD. Masses and ages were determined for the cases with and without rotation, obtaining an average age for the RSGs of 8 Myr, thus doubling the age of the host cluster determined from the pre-main sequence (PMS).

In the final part, it is presented a brief discussion about the discrepancy of the age of Westerlund 1 measured with the PMS isochrones and the age of the RSGs, as well as the uncertainties it raises regarding the formation history of the cluster.

List of Figures

List of Tables

Contents

Chapter 1

Introduction

1.1 *Westerlund 1*

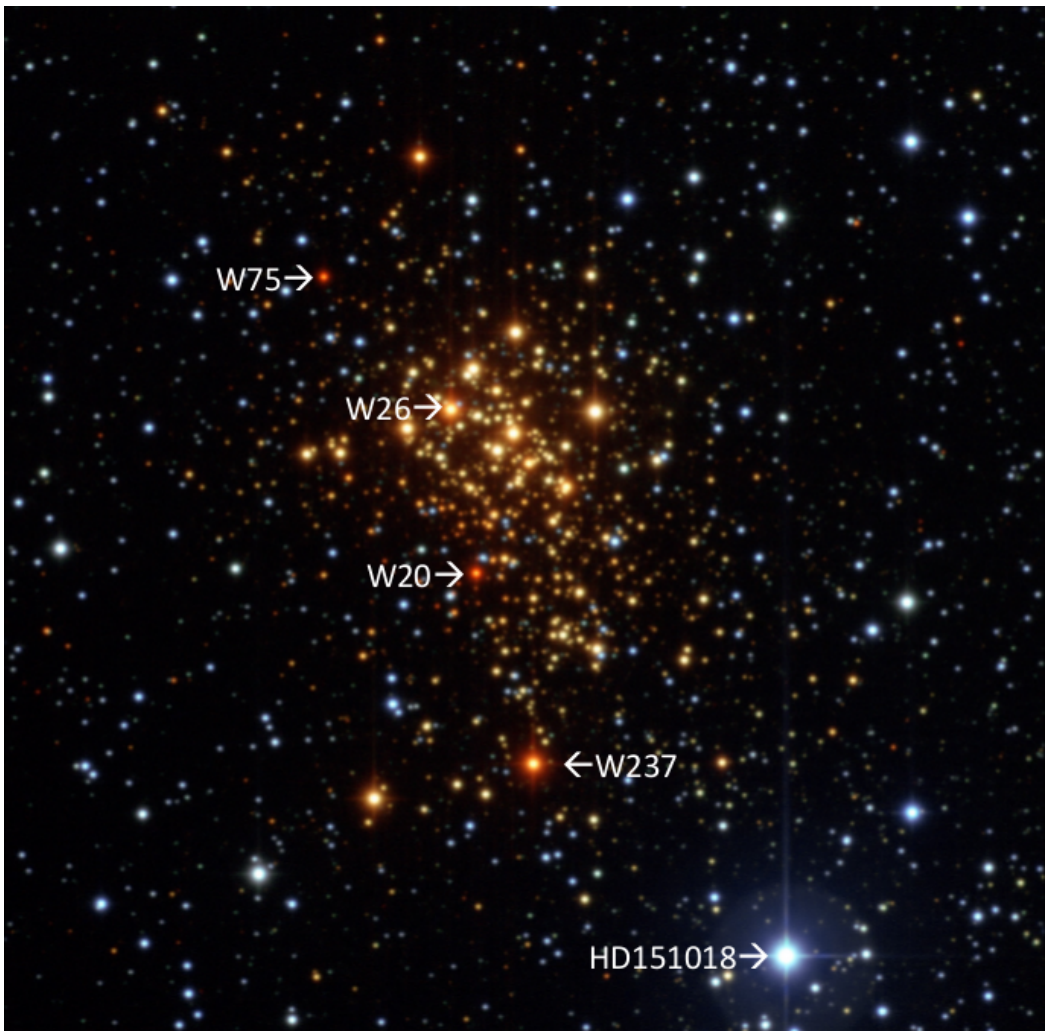

Figure 1.1: Finding chart for Westerlund 1, where the RSGs and the foreground star HD 151018 are indicated. This image was taken from the ESO site: https://www.eso.org/public/images/eso1034c/.

1.1.1 General description of the cluster

Young massive stellar clusters (YMCs), with their age, distance and reddening well constrained, are perfect laboratories that provide a statistically robust sample of stars and allow us to explore more deeply into their evolution.

Westerlund 1, thanks to recent near and mid-infrared surveys, has become one of the most interesting YMCs in our Galaxy. Due to its high mass nature -of the order of $10^5 M_\odot$, see Clark et al. 2005 and Brandner et al. 2008- and its subvirial state (velocity dispersion lower than 4.6 km s^{-1}, see Clark et al. 2014) it is likely to evolve into a Globular Cluster. It represents a unique opportunity to try and answer many questions about the nature of star clusters and also the physical processes taking place during the formation and evolution of massive stars, a subject that is highly filled with uncertainties. Nonetheless, it is well known that massive stars are responsible for plenty of energetic phenomena that enrich the interstellar medium such as: supernovae, gamma-ray bursts and X-ray binaries, thus playing a central role in the evolution of galaxies (Clark et al. 2015).

Unlike other resolved YMCs, Westerlund 1 has an unprecedented population of blue supergiants and yellow and blue hypergiants (YHGs, BHGs and BSGs), whose extensive mass loss is required for the formation of Hidrogen-depleted Wolf Rayet stars (WR). It also has red supergiant stars (RSGs) (see figure 1.1), so we have a diverse population of stars to explore different evolutionary paths.

If a Kroupa IMF is assumed, the mass estimate of $\sim 10^5 M_\odot$ for this cluster is a lower limit, as it has been calculated considering only massive stars (around 200) with masses $\geq 25 M_\odot$ and leaving out the binaries (Negueruela et al. 2010). Nonetheless, lower mass stars in Westerlund 1 can also be considered here, yielding an IMF consistent with standard down to 2 $M_\odot$ (Negueruela 2010)

1.1.2 Formation of Westerlund 1

The cluster presents a homogeneous and co-eval population of about 5 Myr, so it must have formed in a nearly instantaneous starburst. In fact, observations in the lower mass end of the mass function suggest an age spread of less than 0.4 Myr (Clark et al. 2015).

Other star-forming galactic and extragalactic regions show some level of hierarchy, that is, star clusters form in larger complexes embedded within giant molecular clouds. However,

wide field optical imaging of the cluster shows no evidence of hierarchical formation and no satellite clusters. On the other hand, there is no statistical evidende from radial velocity data that it is being formed by the merging of smaller sub-clumps. Also, Westerlund 1 does not seem to be sorrounded by isolated, contaminating massive stars and, in fact, there is evidence for mass segregation (Brandner et al. 2008). All of that suggests that the cluster is likely to have formed in a single, compact and spatially isolated starburst, that is, in monolithical formation.

1.1.3 Binary stars

Westerlund 1 is also a great target to study binary systems and about 70 confirmed and candidate binaries have been identified (Clark et al. 2015). Binary interactions play a central role in stellar evolution, and they are a key to explain why, in Westerlund 1, there is an homogeneous population of OB massive stars while the population of more evolved transitional and Wolf Rayets (WR) stars is more diverse: 23 confirmed WR of which 8 are WC stars and 15 are WN (Crowther et al. 2006).

There are two cases to be discussed regarding how binary systems affect stellar evolution. In the first one, binary interactions have the effect of removing the hidrogen layer of the primary star, making it go through extreme mass-loss and skipping the cool supergiant phase to initiate the WR phase earlier. Meanwhile, the mass that is lost is accreted in part by the secondary star or ejected away. The result of this process is that with hidrogen depleted WRs, we have low mass pre- super nova cores that will likely end up forming neutron stars or magnetars.

In the second case, when there is rapid rotation of massive binaries that leads to highly efficient internal mixing and chemically homogeneous evolution, the mass of the system remains inside the Roche lobe avoiding loss. This eventually leads to a high mass pre-SN core that is expected to end up forming a black hole (BH).

In Westerlund 1, we can find examples such as the supergiant B[e] binary Wd1-9 for the first case scenario, and the blue hipergiant Wd1-5, for the second one. A magnetar has also been detected in the cluster.

1.1.4 Open Questions and perspectives

The particular nature of Westerlund 1, in addition to its diversity of stellar constituents and physical processes triggered among them, raises a lot of questions that are yet to be answered by upcomming observations and theoretical modelling. One of the questions in need for an answer is why Westerlud 1 is currently in a subvirial state when it would be expected to be dynamically relaxed and in virial equilibrium given its radial extent of only about 2 pc (Clark et al. 2015).

Another question that rises is regarding the process by which such an ammount of mass was accumulated in such a small volume of space, since $\sim 10^5 M_\odot$ for a region with a radius of ~ 2 pc gives quite a dense cluster, much denser than R136 in 30 Doradus, for example.

Astronomers would also like to understand what led to the apparently instantaneous formation of Westerlund 1 in an isolated region of the Milky Way, where not much of star formation is seen. As was stated before, this cluster is thought to have originated by monolithical formation.

Also intriguing is the coexistence of RSGs and WRs, which is somewhat unexpected because, at the age of the cluster ($\sim$ 5 Myr) WRs should start disappearing, while it is too early for the RSGs to show up, as they form after 6 Myr (Negueruela et al. 2010).

While these questions are complex and will probably need a lot of time to be answered, there are some problems that can be solved more directly. Ongoing efforts are seeking to construct an HR diagram for the cluster, potentially allowing to constrain the evolutionary paths for supergiant stars. That means an HR diagram would help determining if BSGs, BHGs and YHGs are progenitors or descendants of RSGs. Also, there is research focused on other tasks, such as constraining the distance to the cluster and determining the origin of its high energy emission -it has GeV and TeV gamma ray emission-. Equally important are the efforts to estimate and constrain the rate of mass-loss throughout the full evolutionary cycle of massive stars by measuring the dust content of YHGs and RSGs winds (Clark et al. 2015).

So as it can be seen, the importance of these matters lies in the fact that they would provide answers regarding the nature of Westerlund 1, and also the physical processes that occur in other star formation regions and extragalactic super star clusters that cannot be resolved into individual stars. Besides, the study of Westerlund 1 will give us insights into

the recent star formation history of the Galaxy.

1.2 Red Supergiants

The present work will focus in the Red Supergiants (RSGs) of Westerlund 1, so that an introduction to the nature of this type of stars is presented in this section. The motivation to study the RSGs in this cluster is due to the rare oportunity of finding 4 objects of this kind in the same cluster, whose distance and reddening are well known. Furthermore, they are very bright in the near infrared (NIR), allowing studies in high and mid- spectral resolution and photometry with modest telescopes.

1.2.1 An introduction to Red Supergiants

A comprehensive understanding of massive stars and their evolution is critical to multiple fields in astronomy, and they play a very important role in the understanding of stellar physics, star forming galaxies, supernovae and the chemical enrichment history of the universe. One particular stage of the evolution of massive stars is the one constituted by red supergiants (RSGs), which are helium-burning stars that evolve from main sequence stars with masses in the range of $\sim (8-40)M_{\odot}$. They are an extreme phase in stellar evolution as they are the coldest and largest massive stars, and the most luminous cool stars in the universe that can also have extreme deaths by collapsing to blackholes or Type II-P supernovae, producing neutron stars. For higher mass RSGs, mass-loss can turn them into a transition phase for stars that will die in a later phase of evolution (Levesque 2017).

Stars are classified as RSGs according to some observational criteria and they can be K-type or M-type cool supergiants. Cutoffs in absolute magnitude and color index put RSGs in the upper right corner of the color-magnitude diagram, with effective temperatures between 3500 K and 4500 K, bolometric luminosities of the order of 10^4 $L_{\odot}$ (at least in the Milky Way) and radii from about 100 $R_{\odot}$ to 1000 $R_{\odot}$.

Mass-loss is a key process that occurs in massive stars that affects their evolution. These stars are able to lose more than half of their mass after they come out of the main sequence with most of this loss occurring during the RSG phase (Levesque 2017). This is why RSGs are known for having wide dust envelopes that makes them the dominating dust production objects in young stellar populations, contributing to chemical enrichment

of the interstellar medium. This mass loss also explains why some RSGs eventually evolve to yellow supergiants (that is, they evolve back into YSGs) or Wolf-Rayet (WR) stars.

Whether a RSG star evolves directly into a supernova or evolves blueward on the HR diagram, back to warmer temperatures, depends on different factors such as metallicity, binary evolution, mass loss and initial rotation rate, so it is hard to determine the necessary mass a RSG needs to take a determined evolutionary path. Only low-mass RSGs with less than 17 $M_{\odot}$ have been observationally confirmed as supernovae progenitors, mainly Type II-P or hydrogen rich supenovae (see Smartt 2015), and the reason for this is still unclear. It could be that higher mass RSGs are collapsing directly into black holes, are not being detected by the available surveys, are difficult to capture due to their extended circumstellar dust or they are actually evolving to later phases (YSGs or WRs), which in turn can also explode as supernovae.

Observing RSGs is also useful for extragalactic stellar astrophysics being that this type of stars has extremely high luminosities (10^4 $L_{\odot}$) and are very bright in the optical and the near-infrared. This allows astronomers to obtain moderate resolution spectroscopy out to $\sim$ 3 Mpc and make detections to distances up to tens of Mpc, well beyond the Local Group. Given that RSGs have been formed recently, they can be used as metallicity indicators helping us know how the latter influences massive stellar evolution. This is particularly important to study the galaxies of the early universe, where modeling metal-poor massive stars is fundamental.

So here we have that RSGs are objects that make up a very interesting cross-disciplinary niche and with the upcomming generation of Extremely Large Telescopes and the instruments accompanying them, the possibility to obtain deeper and better observations of RSGs is going to be improved, as well as the current knowledge about stellar evolutionary theory.

1.2.2 Inside a Red Supergiant

1.2.2.1 Evolution and the stellar core

Figure 1.2 shows the evolutionary track of a $15M_{\odot}$ single non-rotating star with solar metallicity. Its pre-RSG evolution consists in going through the main sequence fusing hydrogen (1), mostly via the CNO cycle, increasing its luminosity as a consequence of the

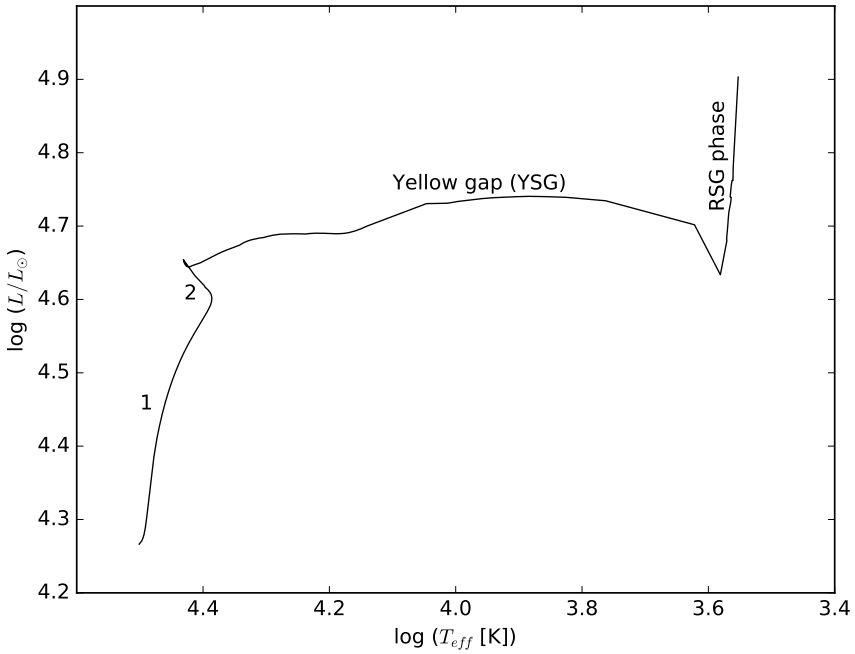

Figure 1.2: Evolutionary track of a non-rotating solar-metallicity $15M_\odot$ star. It was calculated based on the grids of stellar models by Ekström et al. 2012.

μ-effect, which means that as H is burned into He, the mean particle mass μ increases and with it, also the luminosity, according to the mass-luminosity relation derived for such a star: $L \approx \frac{\mu^4}{\kappa} M$. According to $L \propto R^2 T_{eff}^4$, as luminosity increases the stellar radius expands (as a response to a decrease in central pressure while in hydrostatic equilibrium) and T_{eff} suffers a sligth decrease.

By the time ending the main sequence and due to convective mixing, H burning in the core ceases abruptly and the core suffers a contraction that increases the temperature inside the star, while luminosity remains nearly constant (2). This contraction stops when a shell of material surrounding the core reaches the right temperature and density to start fusing hydrogen. While H fusion occurs, the shell contracts and gets to the temperature and density needed for core He fusion. This process produces the so called *mirror effect*, which consists of an expansion of the stellar envelope while the core is contracting. This opposite behavior of envelope and core is explained by the need to maintain the temperature and energy generation rate of the fusion shell.

With the envelope expanding rapidly and the luminosity maintained constant, there has to be an important decrease in T_{eff}. This is where the star is found to be in the very

short Yellow Supergiant (YSG) phase, which lasts about 10^4 years. This short lifetime is why only very few of these stars are found in massive stellar populations. This phase is shown as the nearly horizontal line in the evolutionary track of Figure 1.2.

Finally we get to the RSG phase (the nearly vertical right end in the evolutionary track). This phase begins when the star begins core He fusion. At this point, the star has an effective temperature as low as $\sim 3500 - 4000K$ and an increased radius of more than $100R_{\odot}$, but is as luminous as when it left the main sequence. During the RSG phase, the core burns He producing C and O through the triple-α process for about 1 or 2 Myr (for a $15M_{sol}$ star). Just as H burning in the main sequence, now the star suffers an increase in luminosity due to the increment of the mean particle weight μ. Nonetheless, this time there is no decrease in T_{eff}.

During core He fusion some low mass RSG stars ($\lesssim 12M_{\odot}$) may go through a *blue loop*, that is, they evolve back temporarily on the HRD to the YSG phase and then return to the RSG phase. The physical reasons for this are not well known but may respond to an opposite to the *mirror effect* mentioned previously: while the He fusion core expands, the H shell and the envelope contract leading to an increase in T_{eff}. This blueward evolution is determined by the gravitational potencial of the core ($\Phi_c \sim M_c/R_c$), which depends on the core mass and radius and, when below some critical -and unknown- value, causes the star to go through the *blue loop*. As might be expected, the occurrence of *blue loops* depends on different factors such as: convective overshooting and mixing, rotation, metallicity and mass-loss rates.

During He burning, besides core fusion (and H shell fusion), there is another process that comes into play in the most central regions of RSGs and makes an important contribution to the abundance of heavier elements in the Galaxy. This is the s-process or slow capture process, that occurs when atoms of any of the elements already present during He fusion capture neutrons to form heavier elements. In massive stars, such as RSGs, the constant source of neutrons is ^{22}Ne and the *weak* s-process takes place.

After He core fusion is done in a RSG, the C core fusion starts and a He shell forms around it, in addition to the H shell. With later fusion phases, the star is structured according to the *onion skin* model, with subsequent layers of heavier and heavier elements until a Fe core has formed. As of C core fusion, higher mass RSGs are expected to evolve back to warmer temperatures, but not as YSGs as was the case for some stars during He

fusing, but as Blue Supergiants or Wolf Rayet stars, which have lost their most external layers due to mass loss.

It is important to note that the internal structure of RSGs is very different from the ones of red giants (in spite of the similar name) and asymptotic giang branch stars (AGBs). Red giants and AGBs evolve in a different manner and have smaller initial masses ($\lesssim 8M_{\odot}$). They form degenerate cores and also, are not able to fuse elements heavier than carbon due to the reduction of the core mass caused by dredge-ups that bring the fusion products to the stellar surface. Also, these stars end their lives as planetary nebulae and white dwarfs instead of supernovae. However, there are presumably *Super-AGB* stars (so far, there are only candidates according to van Loon 2017) that are capable of fusing C and causing core collapse supernovae, given a sufficienty high stellar mass.

1.2.2.2 Envelopes and Atmospheres

Besides their core, RSGs also have convective envelopes made up of convective cells, which size is of the order of the stellar radius itself and with this, one could say that RSGs are almost completely convective. According to the mixing length theory, the size of convective cells is determined by the atmospheric pressure scale height H_p of the star. However, according to Chiavassa et al. 2009, in order to reproduce the size of the convective cells in RSGs the turbulent pressure must be taken into account, since it can dominate the gas pressure inside convective layers. With this extra factor, the standard pressure scale height $\left(H_p = \frac{kT_{eff}}{g\mu m_H}\right)$ changes to: $H_p = \frac{kT_{eff}}{g\mu m_H}\left(1 + \beta\gamma(\frac{v_{turb}}{c_s})^2\right)$, where v_{turb} is the turbulent velocity, c_s is the sound speed, γ is the adiabatic exponent, and β is a parameter depending on the anisotropy of the velocity field. This agrees with observational measures of the convection cells, as Chiavassa et al. 2010 shows.

Envelopes in RSGs are very interesting due to their complexity and also extremely difficult to model and hence, understand. Two fundamental reasons for this can be named: supersonic convective flows and differential rotation. The first ones produce acoustic waves that, when arriving at the envelope, make the standard asumptions of mixing length theory and local thermodynamic equilibrium difficult. The second one, originated by the drop in rotation rate of the envelope as it is expanding while the core is contracting, gives rise to magnetic fields that can drive mass loss processes. Nonetheless, codes like *MARCS* or *PHOENIX* produce one-dimensional spherically symmetric stellar atmospheric models

with a good level of agreement with observational spectra in the optical and IR. Such codes assume local thermodynamic equilibrium and use mixing length theory. Also, 3D codes like *CO5BOLD* are being developed, see Chiavassa et al. 2011.

1.2.3 Physical Properties of Red Supergiants

1.2.3.1 Spectra of Red Supergiants

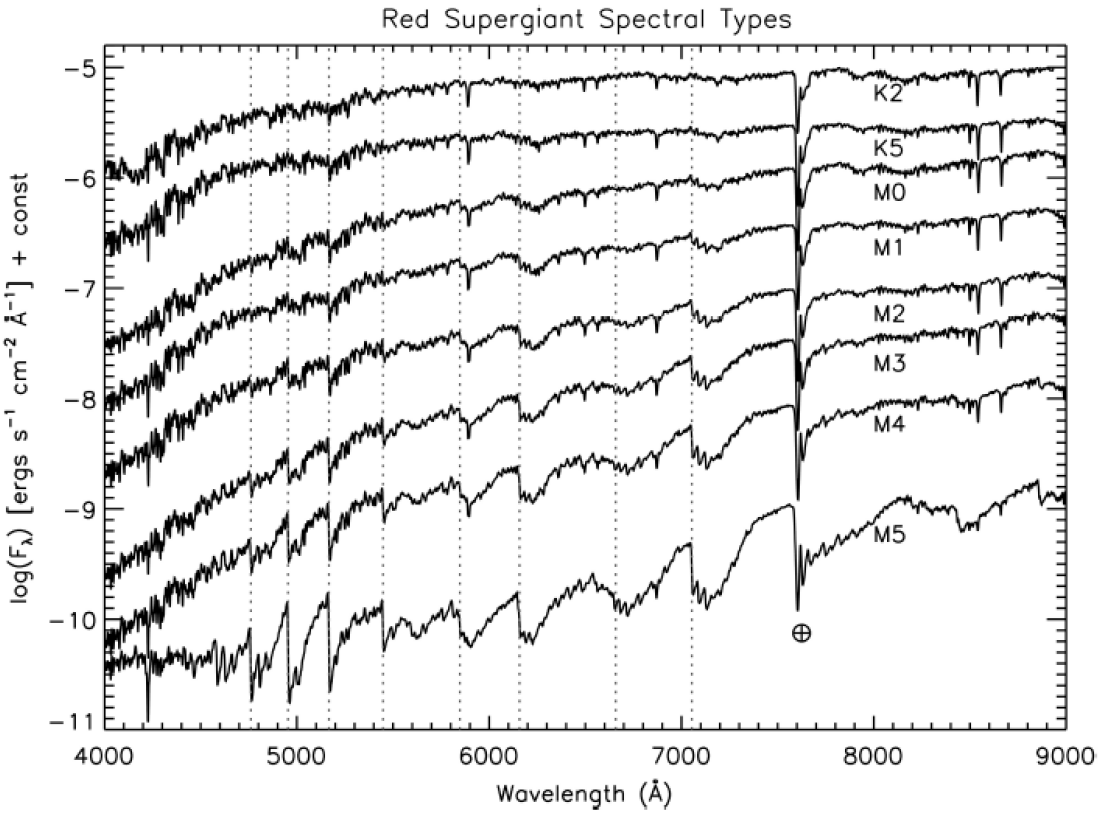

Figure 1.3: Spectral energy distributions of RSGs in the Milky Way. From top to bottom, SEDs go from early K to late M spectral types. The vertical dotted lines mark the TiO bands. This plot was taken from Levesque 2017.

Spectra from RSGs are not easily related to black body spectra because of the line blanketing that increases with later spectral types, and makes it difficult to recognize the emission peak at about 6750-8550 Å for RSG stars in the Milky Way. For this reason, spectral types of RSGs are decided by the strength of certain spectral lines and the presence of molecular bands in the optical regime, especially TiO absorption bands, which start appearing at the spectral type K5 and at later M types they become so deep that

eventually erode the continuum completely. The strength of this feature is the most important one when it comes to determining RSG spectral types later than K5 (see figure 1.3) and, as it will be explained later in this work, together with stellar atmosphere models they are useful to determine effective temperatures.

For earlier K-type RSGs, the determination of the sub-types is more difficult due to the absence of features that evolve with spectral type or that are strong enough to show some utility in spectra with low S/N. The most used features to classify early K supergiants are the CH G-band at 4300 Å, which is weak anyway, and also the shape of the continuum, which reliability might depend on the amount of circumstellar dust surrounding the RSG. In the near-IR regime, spectra are also well characterized by molecular bands, this time the CN band at $1.1\mu m$ and the CO at $2.3\mu m$. Other useful features in the optical and near-IR are the Fe I and Ti I atomic lines, which can be used as temperature indicators for F and G type stars, while for K and M types those are not so reliable (Dorda et al. 2016). When it comes to the ultraviolet (UV) regime, emission at this wavelengths is low compared to the ones at the optical and near-IR, so individual RSGs are not usually studied here.

1.2.3.2 Effective Temperatures

Since most of the radiation emitted by RSGs is in the infrared, their cool temperatures imply significant bolometric corrections that make their luminosity determination highly dependent on effective temperature. Thus, T_{eff} is surely the most important parameter to the characterization of RSGs

Effective temperature refers to the temperature at the place, or radius, in the stellar atmosphere where the opacity (κ) dependent optical depth (τ) is equal to 1. The minimum T_{eff} of stars in hydrostatic equilibrium defines the Hayashi limit, which is cooler at higher metallicities (Levesque et al. 2006, Drout et al. 2012).

The determination of an effective temperature scale that maps T_{eff} to spectral type has been a complicated job mainly because of the scarcity of data from RSGs. Also, the particular characteristics of these stars discard temperature scales obtained for red giants. Temperature scales based on broadband colors, mainly $(B-V)_0$, failed at this task because of this color's sensitivity to surface gravity that ows to line blanketing effects in the B-band, and also the effects of reddening on the continuum, expected in RSGs due to their notable amount of circumstellar dust. The first effective temperature scales for RSGs in

the Milky Way and the Magellanic Clouds yielded temperatures colder than the Hayashi limit, e.g. Humphreys and McElroy 1984.

A better way to determine effective temperature scales for RSGs takes advantage of the TiO features, with deeper molecular bands corresponding to cooler effective temperatures and, as mentioned before, later spectral types. In the context of galaxies or populations with red dwarfs and red giants, the relative young age of RSGs would assure that the TiO abundaces are directly linked to T_{eff} instead of surface metal enrichment over time. And thanks to the improved *MARCS* stellar atmosphere models where opacity effects for oxygen-rich molecules are accounted for, it is now possible to use TiO bands directly to determine the T_{eff} and hence to develop a more reliable temperature scale for RSGs. For example, in the works by Levesque et al. 2005 and Levesque et al. 2006 temperature scales were determined for RSGs in the Milky Way and the Magellanic Clouds respectively, that yielded effective temperatures warmer than the Hayashi limit and hence, better adjusting to predictions of stellar evolutionary models.

Unlike $(B-V)_0$, the $(V-K)_0$ color provides a good alternative to determining the T_{eff}, thus complementing the results provided by the stellar atmosphere models. Calibrations for T_{eff} are available to various metallicities (See the works by Massey et al. 2009, Levesque et al. 2005 y Levesque et al. 2006) under the form:

$$T_{eff} = A - B(V-K)_0 + C(V-K)_0^2 + D(V-K)_0^3 \tag{1.1}$$

Levesque et al. 2005 gives the coefficients for this relation in the Milky Way: $A = 7741.9$, $B = 1831.83$, $C = 263.135$ and $D = 13.1943$, as well as the validity of the calibration over the range $2.9 < (V-K)_0 < 8.0$, (3200 K - 4300 K) with a dispersion of 11 K by considering surface gravities from log g = -1 to 1. In the works by Levesque et al. 2005 and Levesque et al. 2006 these color-temperature calibrations agree with T_{eff} determinations from TiO bands (using *MARCS* models) to within $\sim 100K$.

It is worth mentioning that whatever method is used to determining an effective temperature scale for RSGs, the results are going to be affected by the photometric and spectroscopic variability of these stars.

1.2.3.3 Masses

Given that RSGs usually go through heavy mass-loss processes as they evolve, it is more practical to work with their initial mass. The lower limit for it is about $8M_{\odot}$, although at this point it is difficult to separate observationally low-mass RSGs from super-AGB stars. On the other hand, there is still not an exact initial mass upper limit, but in theory it is defined by the atmospheric Eddington limit, which states that the maximum luminosity that a star can reach so that the radiation pressure does not exceed the gravitational force is given by:

$$L_E^{atm} = \frac{4\pi cGM}{\kappa_{atm}} \tag{1.2}$$

where κ_{atm} is the maximum opacity in the atmosphere over optical depths going from 10^{-2} to 10^3, see Levesque 2017.

According to Ulmer and Fitzpatrick 1998, hot ($> 10^4 K$) and massive ($> 40M_{\odot}$) stars become unstable against radiation pressure and as they come closer to L_E^{atm}, this instability gives place to very intense mass loss by which the stars stop evolving rightward on the HRD and hence, never become RSGs. In fact, observational evidence from the Milky Way and the Large Magellanic Cloud exhibit the lack of presence of luminous cool stars with initial masses between 50 and 60 $M_{\odot}$, that is, such massive stars lose an important amount of their mass before getting to the RSG phase. This would be the case of Luminous Blue Variables (LBV).

1.2.3.4 Luminosities

Luminosity works as a representation for mass, as seen in equation 1.2. However, in the RSG phase when stars begin fusing He, there is a degeneracy where different initial masses lead to an overlap of the evolutionary tracks in the Hayashi line region, that is, an overlap in luminosities.

Knowledge of distances and temperatures of RSGs are key to accurate luminosity determinations. The first is necessary to calculate the distance modulus and the second is used to obtain the bolometric corrections. For these calculations it is better to use K band magnitudes because RSGs are usually not variable in this band. On the other hand, they are variable in the V band.

Bolometric corrections in the K band can be calculated from T_{eff} using expressions of the form:

$$BC_K = A - B(T_{eff}/1000K) + C(T_{eff}/1000K)^2 \tag{1.3}$$

which coefficients depend on metallicity and are obtained from stellar atmosphere models, such as *MARCS*. According to Levesque et al. 2005, coefficient values for the Milky Way are $A = 5.574$, $B = 0.7589$ and $C = 0$. Also, this expression is valid over the range (3200 K - 4300 K) with a dispersion of 0.01 mag by considering surface gravities from *log* g = -1 to 1.

According to the atmospheric Eddington limit (1.2), the maximum luminosity should depend on metallicity, just as the maximum mass, so lower-metallicity (or lower κ_{atm}) RSGs would have higher masses and luminosities, although as stated by Massey et al. 2009, this is not what observations of RSGs in the Local Group have shown and this might be caused by several reasons, among them the following: foreground contamination of YSGs, which would keep out the warmest RSGs from the sample and mass-loss processes that make luminosity calculations difficult due to circumstellar dust. Also, rotation and binarity could have effects over how much a RSG evolves up the Hayashi track.

Just like with the lower mass limit for RSGs, the lower luminosity limit is difficult to determine owing to the contamination by the most luminous lower-mass red giants and AGBs. Still, stellar evolutionary tracks provide an estimated limit of $log(L/L_\odot) \sim 4.0$ and $log(L/L_\odot) \sim 4.5$ for RSGs in the MW and the SMC respectively (Levesque 2017), where there should be little exclusion of lower-mass RSGs and little contamination from red giants and AGBs.

1.2.3.5 Radii

Radii of RSGs can be measured with near-infrared and optical interferometers or can be calculated by the simple luminosity-effective temperature relation $L = 4\pi R^2 \sigma T_{eff}^4$ (black body approximation). Using interferometry to determine radii is observationally challenging because of the small number of neighboring RSGs and is also dependent on the definition of the stellar surface.

RSGs in the Milky Way have radii that span from about $100R_\odot$ to $1500R_\odot$. With these large radii, these type of stars are expected to have superficial rotation rates as low as $< 1\ km\ s^{-1}$. Nonetheless, rotation rates at deeper layers would be determined by

the physical properties of convective layers and fusion shells, giving place to differential rotation.

1.2.3.6 *Surface gravities*

RSGs have extremely low surface gravities that range between $\log g = -0.5$ and $\log g = 0.5$. There are a few ways we can distinguish RSGs from other cool stars with lower luminosities (and therefore higher surface gravities) by using the effects of surface gravity on the SED as a whole, or on individual spectral features. One of such ways is to use the (B-V) vs. (V-R) color-color diagram where, as shown in Figure 1.4, it is possible to observe a clear separation between RSGs and high-gravity red dwarfs, with the first ones being redder due to line blanketing, which diminishes the blue regions of the spectrum in stars with low surface gravities and also the reddening caused by circumstellar dust. Effects of surface gravity on the SED are also possible to identify by fitting observed spectra to synthetic ones.

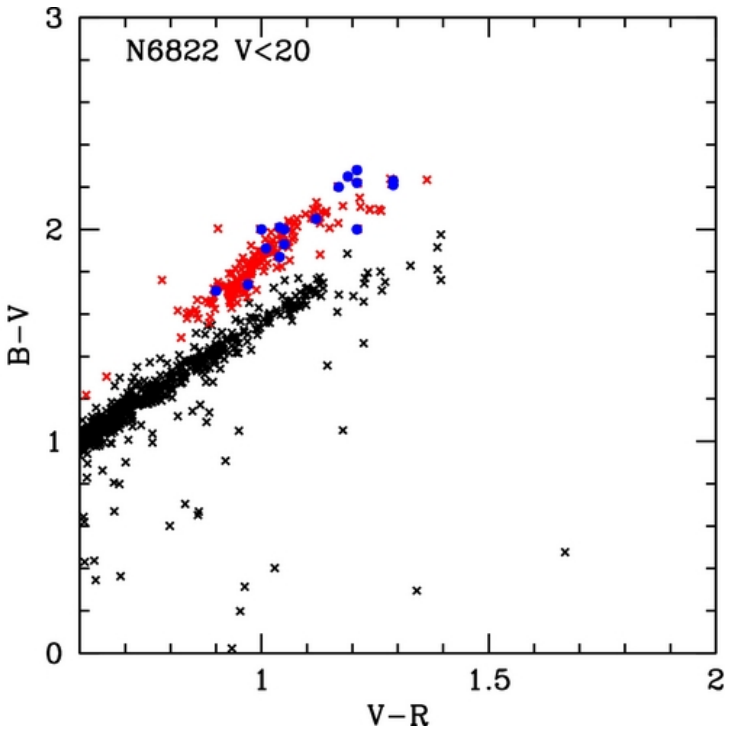

Figure 1.4: (B-V) vs. (V-R) Color-color diagram for Local Group galaxy NGC 6822 that shows the clear separation of RSGs (red points) and foreground dwarfs (black points). RSGs have redder (B-V) colors. This image was taken from Levesque and Massey 2012.

However, the most precise and effective way of discriminating stars by their luminosity

class, allowing us to separate supergiants from giants is by analyzing certain spectral features. For instance, the Ca II triplet lines (8498, 8542, 8662 Å) are highly sensitive to surface gravity getting stronger with lower log g, but they are also dependant on metallicity and T_{eff}. In that case, the $H\alpha$ absorption line (6563 Å), though weak in RSG's, makes up an alternative option that is not so sensitive to those.

1.2.4 Red supergiants in and beyond the Milky Way

1.2.4.1 Identifying red supergiant populations

In principle, the most straightforward manner to identify RSGs is by taking their photometric magnitudes to plot them in a magnitude-color diagram, yielding direct information about their effective temperature and their luminosity. Several criteria for identifying RSGs with photometric data have been proposed, for example for UBVRI data, Massey 2002 identified a population of RSGs in the Magellanic Clouds with magnitudes between $V = 14$ and $V = 12$ and color ranging from $B-V = 1.5$ and $B-V = 2$; Massey and Olsen 2003 found, also in the Magellanic Clouds, a sample of RSGs with $(V - R)_0 \geq 0.6$; for near and mid-infrared photometry, which comes to be very useful when observing targets located at high-extinction sightlines, works such as González-Fernández et al. 2015 have used cutoff criteria based on the $(J - K_s)$ and $(H - K_s)$ colors and the K_s magnitude. Britavskiy et al. 2014 proposed criteria using also 3.6 μm and 4.5 μm photometry together with JHK bands to identify RSG populations.

In spite of those works, the plain use of colors and magnitudes fails to identify distant red sources because of the contamination of foreground red giants and dwarfs, which makes it difficult to distinguish them from RSGs. As mentioned in section 1.2.3.6, there is a simple method proposed by Massey 1998 to separate stars with extreme luminosity classes with a cutoff defined by $(B-V) = 1.26 \times (V-R) + 0.45$ that effectively discriminates backgroud RSGs and foreground dwarfs (see Figure 1.4). However, separating lower-mass RSGs from foreground luminous red giants is a different and more challenging problem, in which case the cutoff condition that $M_{bol} < -7.0$ for RSGs (see Massey and Olsen 2003), actually can leave out the lowest-mass RSGs in a given sample. Also, photometric methods might not be useful when trying to remove largely distant backgroud contaminants, for instance, distant luminous red galaxies and globular clusters could misguide RSG identification.

Spectroscopic observations also provide ways to identify RSGs, but as with photometry, none of the existing methods are definitive. Only if the motions of the sources are well-known, it is possible to separate foreground and backgroud samples kinematically, but there are a lot of factors that make this method inefficient. However, as mentioned before, spectral features in the optical and near-IR, such as the Calcium Triplet and the $H\alpha$ absorption line are useful to distinguish RSGs and red giants thanks to their sensitivity to surface gravities. Nonetheless, the analysis of these spectral features with the purpose of RSG identification is not hurdle free.

In the Milky Way only a few hundred confirmed RSGs have been identified out of the $\sim$ 5000 supergiants predicted by Galactic models only for M-type stars (e.g. Gehrz 1989). The best studied stars among them are those in OB associations or clusters at higher Galactic latitudes (and therefore minimal Galactic extinction) and known distances. Recently, more RSGs have been identified at lower latitudes, for example the ones in the five RSG clusters, called RSGC1 to RSGC5, that gather about 76 spectroscopically confirmed RSGs (Clark et al. 2009).

It is feasible to study these massive stellar populations also in other galaxies thanks to their high luminosities, allowing to have insights into how different environments affect stellar evolution. Extragalactic RSGs have been studied especially in the Local Group with a substantial population identified in the Magellanic Clouds. Also, in recent years near-IR spectroscopy has provided J-band spectra for individual RSGs in galaxies beyond the Local Group, spanning a broad range of metallicities.

Metallicity, which has a strong influence over the evolution of massive stars, has a very interesting effect on spectral type and effective temperatures of RSG populations. On one side, different studies (e.g. Elias et al. 1985, Levesque and Massey 2012 and Dorda et al. 2016) have shown a shift to earlier average **spectral types** at lower metallicities, which is not hard to imagine if one keeps in mind that TiO bands must be weaker at environments with lower abundances. Furthermore, observational evidence (e.g Drout et al. 2012) matches with stellar evolutionary models that have predicted a shift to warmer average **effective temperatures** at lower metallicities following the behavior of the Hayashi limit. This might challenge the photometric identification of low-metallicity RSGs due to their average shift to the blue side of the HR diagram.

Metallicity also seems to affect the lifetime a massive star spends in a certain evolu-

tionary phase. For instance, the number of BSGs with respect to the number of RSGs, represented by the blue-to-red supergiant ratio (B/R), decreases with metallicity possibly due to lower mass-loss rates and thus, longer RSG lifetimes (see Maeder et al. 1980). The same behavior is followed by the Wolf-Rayet to RSG ratio (Massey 2002).

1.2.5 Variability in Red Supergiants

1.2.5.1 Photometric variability

There are many physical phenomena that contribute to photometric variability in some RSGs. Changes in their apparent magnitudes and fluctuations in their lighcurves can be caused by one of those phenomena or by a combination of them, so it becomes difficult to establish what are the exact physical origins of variability in a RSG without comprehensive multi-wavelength monitoring, which is hard to carry out.

Normal RSG stars show photometric variability mostly in the optical regime, where typical changes in the V band are about 1 mag. They show far less variability in the near-IR with changes of about 0.25 mag in the K band. Depending on their lightcurves, RSGs are classified as irregular variables and semi-regular variables (SRc). Irregular variables have complex lightcurves that cannot adjust to any period, and semi-regulars are subclassified as *short period*, with periods of the order of hundreds of days, and *long secondary period* (LSP) that have periods of more than 1000 days. Most of variable RSGs are LSP and a few others show a combination of short and long periods in their lightcurves, such as Betelgeuse and μ Cephei. Meanwhile, short period variable RSGs are not as common (Levesque 2017). Causes for photometric variability include the following (Levesque 2017):

- As mentioned in section 1.2.2, the atmospheres of RSGs are formed by giant convection cells that when turning over cause brightness variations, originating Long Secondary Periods (Stothers 2010).
- Episodic or variable mass loss processes can affect the distribution and structure of the circumstellar dust yielding temporary changes in color and increasing spectrum veiling.
- Binary companions can produce photometric variations due to eclipses, mass transfer and wind interactions.

- Radial pulsations also yield brightness variations. However, it is not clear if they take place in all RSGs and are only detected in some of them.

1.2.5.2 Spectroscopic variability

Considering their extended atmospheres and the physical phenomena that take place in them, small spectroscopic variability is perfectly expected in RSGs. All the phenomena mentioned before as causes for photometric variability also contribute to variations in spectral features, so that when determining spectral types, fluctuations of the order of one subtype or less are detected, although they can be attributed to errors, given the qualitative nature of the methods to determine spectral types.

Major spectroscopic variability corresponding to changes of the order of spectral types (one or more), however, has only been detected in a few RSGs. These variations are extreme and rapid and are representative of actual changes in physical properties, like effective temperature. Stars displaying such variations also show important alterations in bolometric luminosity, circumstellar reddening and unusual variation in the V-band (well beyond 1 mag). Stars of this kind are then brighter, dustier and more luminous at earlier spectral types, and at colder types they have been observed to surpass the Hayashi limit evidencing the unsurprising fact that they might be hydrostatically unstable (see Levesque et al. 2007). A clear example of these heavily variable stars is HV 11423 in the SMC, which was classified as K0-1 with a T_{eff} of 4300 K in December of 2004 and a year later was classified as type M4 with a T_{eff} of 3500 K. Subsequent observations have placed this star as a K0-1 type again and then as a M0 I and M1.5, with corresponding effective temperatures (see Massey et al. 2007).

Such a strong variability is still not thoroughly explained but causes include sporadic mass loss, that modifies the opacity in the photosphere and the structure of the circumstellar dust, and low metallicity, which appears to be related to the number of variable RSGs in sub-solar metallicity galaxies (Dorda et al. 2016).

Additionally, there are some RSGs with fixed spectral types, deduced from TiO band strengths, that show variable *emission* features, but this is an area where more studies are needed.

Chapter 2

Photometric Analysis of the Red Supergiants in Westerlund 1

2.1 *Effective temperature determination*

Effective temperatures of the four RSGs in Westerlund 1 were estimated through three different ways using the observed apparent magnitudes listed in table 2.1, that were derredened according to the extinction law determined by Damineli et al. 2016 (see table 2.2).

BVRI magnitudes were taken from Clark et al. 2005 together with averaged measurements at R and I filters carried out at *Observatório do Pico dos Dias* (OPD) between years 2006 and 2014. JHK magnitudes were also obtained at OPD with J, H and K filters, between those same years. All three calculations of T_{eff} used color-temperature calibrations.

	Filter						
Star	B_0	V_0	R_0	I_0	J_0	H_0	K_0
W237	7.31	6.23	5.52	4.08	2.52	2.04	1.70
W20	-	-	8.13	5.68	3.94	3.04	2.50
W26	6.59	5.79	5.18	5.09	2.58	1.87	1.66
W75	-	-	9.38	6.85	4.62	3.39	2.70

Table 2.1 - Derredened apparent magnitudes of the RSGs in Westerlund 1 observed at different filters.

Firstly, T_{eff}'s were calculated by using the color-temperature relationship found by Levesque et al. 2005 for the Milky Way (see equation 1.1). Since V band photometry is only available for two of the stars, it was only possible to calculate T_{eff} for W26 and W237

A_B	A_V	A_R	A_I	A_J	A_H	A_K
15.49	11.26	8.44	5.71	2.34	1.29	0.74

Table 2.2 - Extinction at different filters used to obtain the derredened apparent magnitudes in table 2.1.

with this method.

Then, T_{eff}'s were calculated by using the color-temperature relationship that Levesque et al. 2005 found by means of the *MARCS* models:

$$(J-K)_0 = 3.10 - 0.547(T_{eff}/1000K) \tag{2.1}$$

Lastly, T_{eff}'s were estimated with the help of the color-temperature calibration grid developed by Worthey and Lee 2011 along with their interpolation program. Worthey and Lee 2011 provide an empirical tabulation of seven colors ($(V-K)_0$, $(U-B)_0$, $(B-V)_0$, $(V-R)_0$, $(V-I)_0$, $(J-K)_0$ and $(H-K)_0$) and the V-band bolometric correction BC_V as functions of T_{eff}, log g and [Fe/H]. All these data were obtained from numerous sources and catalogs.

Previous to Worthey and Lee 2011 there had been several synthetic or semi-empirical color-temperature calibrations (e.g. Houdashelt et al. 2000 and VandenBerg and Clem 2003). However, those works are quite vulnerable to errors that can be due to incompleteness and incorrect assumptions in the process of synthesizing spectra and obtaining fluxes from them. Besides, they count on rather insufficient empirical photometric data. Being that the calibration by Worthey and Lee 2011 is entirely empirical, it avoids the problems of synthetic calibrations and still gathers a wider set of photometric data.

By playing with the interpolation program for the calibration grid by Worthey and Lee 2011, values of T_{eff} and BC_V were obtained so that the photometric colors $(J-K)_0$ and $(H-K)_0$ could be as close as possible to the observed ones (see table 2.1). It was not possible to make colors that include the V_0 magnitude ($(V-K)_0$, $(B-V)_0$, $(V-R)_0$ and $(V-I)_0$) agree with the $(J-K)_0$ and $(H-K)_0$ colors, so the V band was not used to obtain T_{eff}'s from the grid in the case of W20 and W75. However, for W26 it was possible to come to an agreement between $(V-K)_0$, $(J-K)_0$ and $(H-K)_0$, and the same happened with $(V-R)_0$, $(J-K)_0$ and $(H-K)_0$ in the case of W237.

In spite of the greater completeness of this grid compared to previous ones, it presents

some gaps that are evident at the time of interpolating data. For example, an extrapolation alert is produced when trying to obtain the color-temperature relation for the star W75, since it appears to be extremely cool, at least according to the JHK photometry. However, the best attempt was made in order to obtain the T_{eff} and BC_V using the grid.

The temperatures found by the three methods just described in this section are summarized in table 2.3. Given the many sources of error, which, for the most part, cannot be determined in this work, *nominal* or lower limits for uncertainties have been estimated and propagated throughout this chapter. With that said: $\Delta A_K = 0.01$; $\Delta V = \Delta J = \Delta K = 0.01$; $\Delta V_0 = \Delta J_0 = \Delta K_0 = 0.014$ and $\Delta(V_0 - K_0) = \Delta(J_0 - K_0) = 0.02$. Errors are propagated thereafter for the stellar parameters.

Star	T_{eff}(K)		
	from $(V-K)_0$ using eq. 1.1	from $(J-K)_0$ using eq. 2.1	from grid
W237	3617 ± 27	4168 ± 37	4250 ± 25
W20	-	3035 ± 37	2650 ± 25
W26	3735 ± 20	3985 ± 37	3750 ± 25
W75	-	2157 ± 37	2200 ± 50

Table 2.3 - Effective temperatures of the RSGs in Westerlund 1.

As it can be seen in figure 2.1, temperatures obtained from $(J-K)_0$ and from the grid are reasonably close with a difference not bigger than $\sim$ 200 K, except for W20. Only in the case of W26, the T_{eff} obtained from $(V-K)_0$ is pretty close from the one obtained from the grid, however, T_{eff}'s obtained with $(V-K)_0$ should not be reliable due to the high variability of RSGs in the V band. Besides, given that V band information is available for only two of the stars, not much can be said at this point except that $(J-K)_0$ gives much higher temperatures than $(V-K)_0$, up to 551 K hotter in the case of W237.

2.2 Bolometric correction and bolometric magnitude determination

After the T_{eff}'s have been derived, it is now necessary to determine the bolometric magnitudes of every star (M_{bol}) and in order to obtain them, the absolute magnitudes and bolometric corrections are needed.

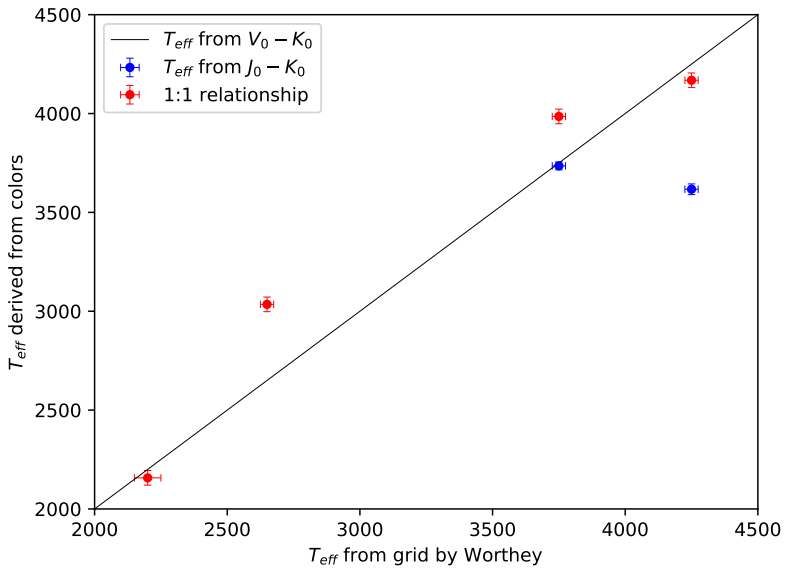

Figure 2.1: Comparison between T_{eff}'s derived from colors and the T_{eff} obtained from the grid by Worthey and Lee 2011.

2.2.1 *Absolute magnitudes*

To calculate the absolute magnitudes of the four RSGs at every filter it is used the distance to Westerlund 1 obtained by Almeida and Damineli 2018 based on the eclipsing binary W36: D = (4.35 ± 0.20) kpc. By using the definition of distance modulus: $M = M_0 + 5 - 5\ log\ d$, where M_0 corresponds to derredened magnitudes (see table 2.1) and d is the distance in pc, the magnitudes in table 2.4 were obtained, all with an uncertainty of ± 0.10 mag.

	Filter						
Star	M_B	M_V	M_R	M_I	M_J	M_H	M_K
W237	-5.88	-6.96	-7.67	-9.11	-10.67	-11.15	-11.49
W20	-	-	-5.06	-7.51	-9.25	-10.15	-10.69
W26	-6.60	-7.40	-8.01	-8.10	-10.61	-11.32	-11.53
W75	-	-	-3.81	-6.34	-8.57	-9.80	-10.49

Table 2.4 - Absolute magnitudes of the RSGs in Westerlund 1.

2.2.2 Bolometric corrections

Since the objects of study of the present work are red stars, it is immediate and practical to want to obtain bolometric corrections at K (BC_K), so it was calculated in six ways that are described below.

First, the expression 1.3 derived from stellar atmosphere models was used with the corresponding coefficients found by Levesque et al. 2005. With this, BC_K was calculated as a function of the T_{eff}'s obtained with $(V-K)_0$ (equation 1.1, only for W26 and W237), with $(J-K)_0$ (equation 2.1) and also with the T_{eff} obtained with the grid by Worthey and Lee 2011.

In the second place, colors $(V-K)_0$ and $(J-K)_0$ are given a special attention in the present work due to the clear trend between NIR colors and spectral type suggested by González-Fernández et al. 2015. So, the work by Bessell and Wood 1984 that proposes a BC_K for late type stars given as a function of the colors $(V-K)_0$ and $(J-K)_0$ (equations 2.2 and 2.3) is used here.

$$\begin{aligned} BC_K &= [20.66 - 19.2(V-K)_0]/[1.0 - 5.5(V-K)_0], \\ 3 &< (V-K)_0 < 14 \end{aligned} \tag{2.2}$$

$$\begin{aligned} BC_K &= 0.72 + 2.65(J-K)_0 - 0,67(J-K)_0^2, \\ 0.6 &< (J-K)_0 < 2 \end{aligned} \tag{2.3}$$

Lastly, BC_K was directly obtained from the BC_V given by Worthey and Lee 2011 following expression 2.4. All the bolometric corrections obtained are in table 2.5.

$$BC_K = BC_V + (M_V - M_K) \tag{2.4}$$

2.2.3 Bolometric magnitudes

Determination of bolometric magnitudes is now straightforward using eq. 2.5. The six M_{bol}'s obtained for every star are shown in table 2.6.

$$M_{bol} = M_K + BC_K \tag{2.5}$$

Star	BC_K obtained from:					
	eq. 1.3, T_{eff} from $(V-K)_0$	eq. 1.3, T_{eff} from $(J-K)_0$	eq. 1.3, T_{eff} from grid	eq. 2.2	eq. 2.3	BC_V in grid
W237	2.83 ± 0.02	2.41 ± 0.03	2.35 ± 0.02	2.77 ± 0.00	2.44 ± 0.03	3.80 ± 0.15
W20	-	3.27 ± 0.03	3.56 ± 0.02	-	3.15 ± 0.01	-
W26	2.74 ± 0.02	2.55 ± 0.03	2.73 ± 0.02	2.70 ± 0.00	2.59 ± 0.03	2.76 ± 0.17
W75	-	3.94 ± 0.03	3.90 ± 0.04	-	3.34 ± 0.00	-

Table 2.5 - Bolometric corrections at K for the RSGs in Westerlund 1.

Star	M_{bol} calculated with BC_K's obtained from:					
	eq. 1.3, T_{eff} from $(V-K)_0$	eq. 1.3, T_{eff} from $(J-K)_0$	eq. 1.3, T_{eff} from grid	eq. 2.2	eq. 2.3	BC_V in grid
W237	-8.66 ± 0.10	-9.08 ± 0.10	-9.14 ± 0.10	-8.72 ± 0.10	-9.05 ± 0.10	-7.70 ± 0.18
W20	-	-7.42 ± 0.10	-7.13 ± 0.10	-	-7.55 ± 0.10	-
W26	-8.79 ± 0.10	-8.98 ± 0.10	-8.80 ± 0.10	-8.83 ± 0.10	-8.94 ± 0.10	-8.77 ± 0.20
W75	-	-6.56 ± 0.10	-6.59 ± 0.11	-	-7.15 ± 0.10	-

Table 2.6 - Absolute bolometric magnitudes of the RSGs in Westerlund 1.

A comparison between methods to calculate bolometric magnitudes is shown in figure 2.2, only in the cases where it was possible to estimate M_{bol} for all four RSGs. Here, it can be seen that when using equation 1.3 in Levesque et al. 2005, both the T_{eff}'s obtained from the grid and the color $(J-K)_0$ (equation 2.1) yield similar results. Also, both the expressions 1.3 and 2.3 suggested by Levesque et al. 2005 and Bessell and Wood 1984 respectively, yield similar results when calculating M_{bol} from $(J-K)_0$.

About the calculations involving the V-band, it is worth noting that M_{bol}'s were obtained with a standard deviation of 0.08 and 0.49 magnitudes for W26 and W237 respectively, meaning that in the case of W26 all six methods yield very consistent results, while for W237, whether it is through $(V-K)_0$ or BC_V, the V band yields much higher M_{bol}'s compared to the ones obtained through the three methods described above and in figure 2.2. Particularly the method that uses the BC_V obtained from the grid to calculate the BC_K, yields a M_{bol} about 1 magnitude higher than the ones obtained from $(V-K)_0$, this means that the grid and the accompanying software do not provide a good estimate of BC_V. All of this suggests that the behaviour of W237 at the V band should be looked at

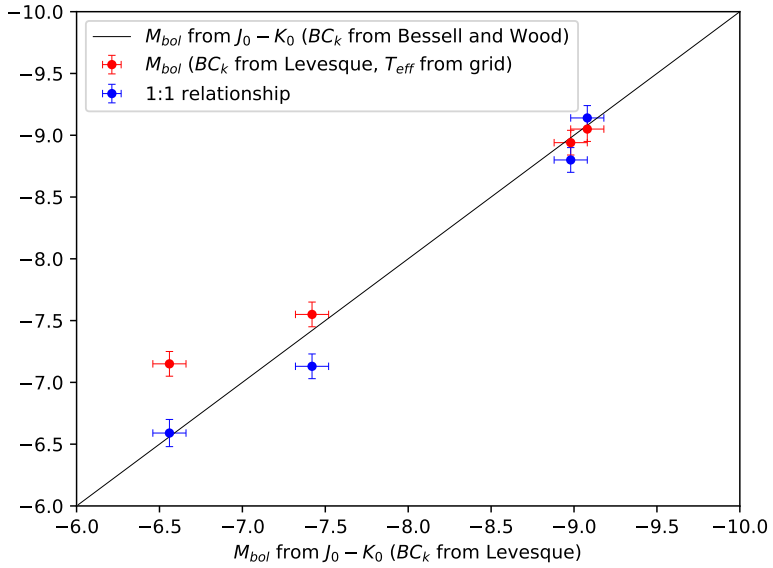

Figure 2.2: Comparison between M_{bol}'s derived from different methods.

carefully.

2.3 Luminosity determination

Luminosity was determined directly from M_{bol} following the relation 2.6. The six luminosity values obtained for every star are given in $10^5 L_\odot$ units, in table 2.7.

$$M_{bol} = M_{bol_\odot} - 2.5log(L/L_\odot), with M_{bol_\odot} = 4.74 \tag{2.6}$$

Star	$L(\times 10^5 L_\odot)$ calculated with BC_K's obtained from:					
	eq. 1.3, T_{eff} from $(V-K)_0$	eq. 1.3, T_{eff} from $(J-K)_0$	eq. 1.3, T_{eff} from grid	eq. 2.2	eq. 2.3	BC_V in grid
W237	2.30 ± 0.22	3.38 ± 0.32	3.58 ± 0.33	2.42 ± 0.22	3.28 ± 0.32	0.94 ± 0.16
W20	-	0.73 ± 0.07	0.56 ± 0.05	-	0.82 ± 0.08	-
W26	2.59 ± 0.24	3.08 ± 0.29	2.62 ± 0.24	2.68 ± 0.25	2.97 ± 0.28	2.53 ± 0.47
W75	-	0.33 ± 0.03	0.34 ± 0.03	-	0.57 ± 0.05	-

Table 2.7 - Luminosities of the RSGs in Westerlund 1, in solar units.

2.4 Radii determination

Radii of the four RSG stars were calculated using the black body approximation stated in section 1.2.3.5. For this, coherent pairs of L vs. T_{eff} were considered, for example, if T_{eff} was calculated from the color $(J-K)_0$, then the BC_K (and hence also M_{bol} and L) was either calculated directly from $(J-K)_0$ (equation 2.3), or through the expression 1.3 using this very same T_{eff}. This way, six different radii were obtained for every one of the four RSGs and are presented in table 2.8.

Radii were obtained with a standard deviation of 59,02 $R_\odot$ for W20, which represents 6 % of the smaller radius that was obtained. For W26 the standard deviation is 31.93 $R_\odot$, about 3 % of the smaller radius obtained. For W75 the standard deviation is 202.78 $R_\odot$, about 16 % of the smaller radius. And for W237, the standard deviation is 228.92 $R_\odot$, which is a considerable deviation when the value of $R = 567.37 R_\odot$ is included, but without it, the standard deviation is only 65.50 $R_\odot$, about 6 % of the smaller value.

Star	Radii (in $R_\odot$) calculated with L's obtained from:					
	eq. 1.3, T_{eff} from $(V-K)_0$	eq. 1.3, T_{eff} from $(J-K)_0$	eq. 1.3, T_{eff} from grid	eq. 2.2	eq. 2.3	BC_V in grid
W237	1223 ± 60	1117 ± 57	1105 ± 53	1255 ± 61	1101 ± 57	567 ± 48
W20	-	981 ± 53	1125 ± 57	-	1039 ± 55	-
W26	1218 ± 58	1167 ± 60	1214 ± 59	1240 ± 59	1145 ± 59	1194 ± 111
W75	-	1303 ± 77	1272 ± 85	-	1716 ± 98	-

Table 2.8 - Radii of the RSGs in Westerlund 1, in solar units.

From the results obtained up to this point, it can be said that all methods yield consistent results, but the BC_K obtained from the grid, directly from BC_V, does not provide a good approximation and is not useful to the calculations in the case of W237. Since the software by Worthey and Lee 2011 does not give any extrapolation warning for this star, the reason for this outsider result must lie in the V_0 magnitude of W237.

2.5 Hertzsprung-Russell diagram with evolutionary tracks

The results obtained so far are summarized in figure 2.3, where the RSGs are plotted in the L - T_{eff} diagram together with the evolutionary tracks in Ekström et al. 2012. As

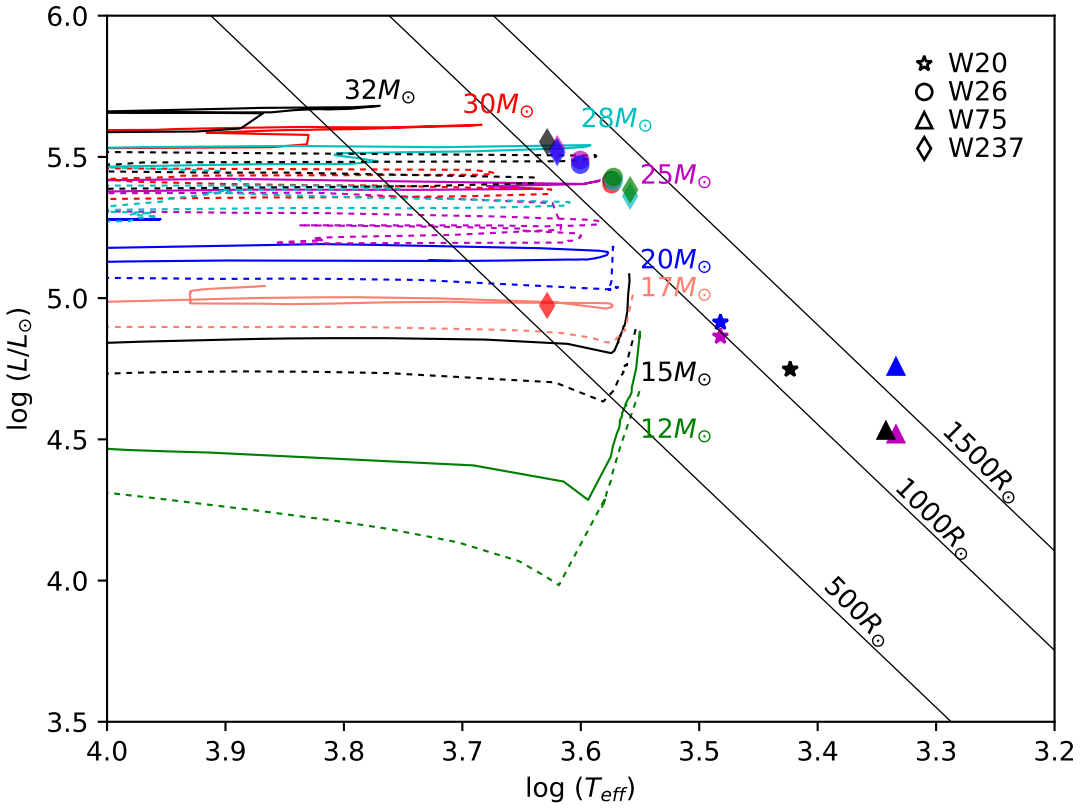

Figure 2.3: Luminosity vs. T_{eff} diagram in *log* units with evolutionary tracks. The tracks are from Ekström et al. 2012. The dotted lines are the no-rotation models and the solid lines are models with initial rotation velocity of $0.4V_{crit}$. Colors link the tracks to the corresponding initial mass. The four RSGs are displayed with the indicated symbols and with colors representing one of the six methods used to obtain the luminosity: Cyan color represents calculations from BC_K in eq. 1.3 and T_{eff} from $(V-K)_0$ (eq. 1.1); Magenta is for BC_K in eq. 1.3 and T_{eff} from $(J-K)_0$ (eq. 2.1); Black is for BC_K in eq. 1.3 and T_{eff} from the grid; Green is for BC_K in eq. 2.2 and T_{eff} from $(V-K)_0$ (eq. 1.1); Blue is for BC_K in eq. 2.3 and T_{eff} from $(J-K)_0$ (eq. 2.1); Red is for BC_K (BC_V) and T_{eff} from the grid. The diagonal lines are the lines of constant radii.

explained in the figure, the different colors of the points represent the six different methods used to do the calculations. Here, it can be seen that W20 and W75 are well far to the right of the evolutionary tracks (right of the Hayashi limit), and since for these two stars T_{eff} was only determined from the color $(J-K)_0$ and from the grid, which at the same time links $(J-K)_0$ and $(H-K)_0$ to T_{eff}, the problem must lie in one, or both, of their infrared magnitudes J_0 and K_0. Also, since BC_K's calculated for these stars all depend ultimately on $(J-K)_0$, the luminosities and radii found are not reliable.

The problem about the color index $(J-K)_0$ has to do with circumstellar dust. Dust may influence the stellar colors in two ways: First, warm dust increases the stellar brightness in the K band yielding a redder color $(J-K)_0$, as if the star had a lower T_{eff}; and second, dust absorption causes extinction that increases strongly towards shorter wavelengths, making the star appear much fainter than normal in the V band and reddening its $(V-K)_0$ color, as if it were a cooler star. Figure 2.4 shows a color excess plot for Westerlund 1 that clearly indicates that the color excess $E(J-K)$ for W20 and W75 is bigger than the average for the cluster, which means that both stars have indeed an excess of emission at the K band. So, these stars have their $(J-K)_0$ color index affected by hot dust emission.

On the other hand and going back to figure 2.3, W26 and W237 show a better agreement with the tracks, which suggest that these stars have initial masses between 25 $M_\odot$ and 28 $M_\odot$. For these two stars it was possible to use $(V-K)_0$ to do the calculations and the results do not differ much from the ones that were made based on $(J-K)_0$ or the grid.

In the case of W26 all six calculations yielded very close results, only with T_{eff}'s and L's calculated from $(J-K)_0$ (blue and magenta points) being slightly warmer and more luminous than the others. As it can be seen, the other four points (in black, red, cyan and green) are very close due to the high consistency of the methods used. In the case of W237 the consistency between the methods is almost as good as for W26, with the only outlier being the red point, with its low luminosity due to the BC_V given by the grid, which is not a reliable data, as suggested in section 2.4.

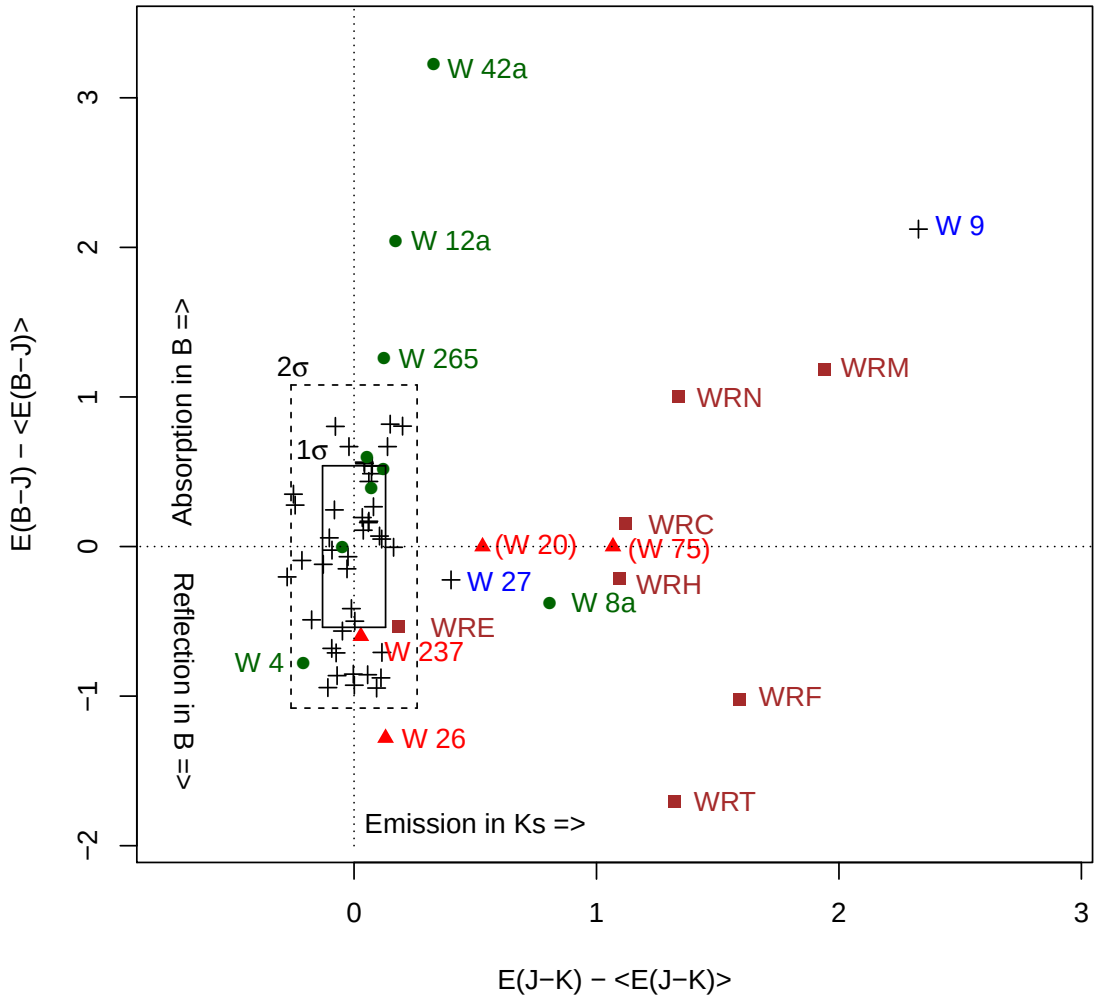

Figure 2.4: Color excess diagram for Westerlund 1 showing the excess of emission at the K band for W20 and W75, which corresponds to their color index $E(J-K)$ minus the average index for the cluster.

Chapter 3

Spectral Analysis of the Red Supergiants in Westerlund 1

3.1 Spectral classification

Near infrared spectra covering the Calcium Triplet (CaT) region from $\sim$ 8400 Å to $\sim$ 8900 Å, of the four RSGs in Westerlund 1, were obtained on *epoch 1*[1] with the Coudé spectrograph and the 1.6 meter telescope of *Observatório do Pico dos Dias* (OPD) and on *epoch 2*[2] with the 4.1 meter *Southern Astrophysical Research Telescope* (SOAR) and its Goodman spectrograph (for details on the observations, see A.1). As an example, the spectra obtained with the SOAR telescope are plotted together with all the features analyzed in this work in figure 3.1, and since it was not possible to obtain spectra for W75 with the SOAR telescope, the one obtained with the OPD telescope is shown. All the analysis described in this chapter was performed with the help of IRAF.

As stated in Dorda et al. 2016, the CaT spectral region is very convenient for the spectral study of RSGs as it provides many advantages over the optical spectral range. For instance, it is close to the emission peak of typical RSGs; it is little affected by extinction and telluric absorption, compared to the optical region; and provides many spectral features useful for spectral classification. However, even though classification criteria in this spectral region for less luminous cold stars have been widely studied by many authors, when it comes to later type supergiants it becomes an unresolved matter,

[1] Hereafter and for the purposes of this work, *epoch 1* will refer indistinctly to any of the epochs when spectra were obtained with this telescope: July 5, 2012 for W26 and W237; July 18, 2013 for W20; and August 7, 2014 for W75.

[2] Hereafter, *epoch 2* refers to July 4, 2017.

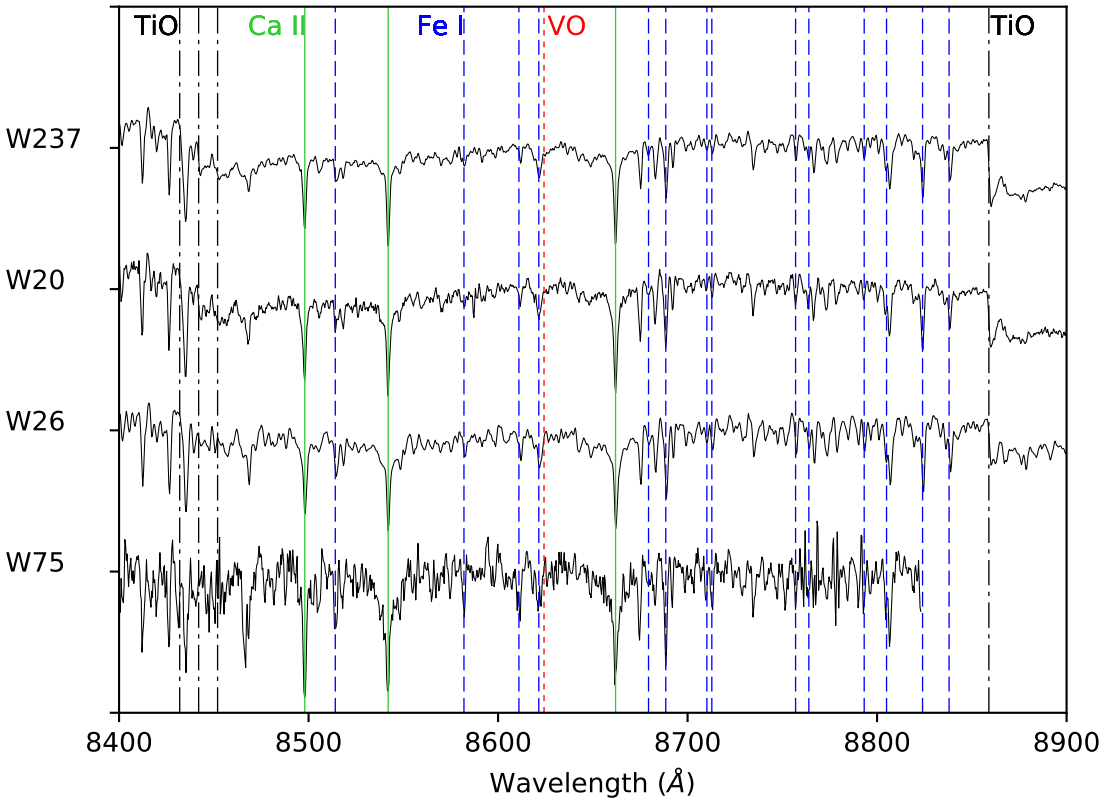

Figure 3.1: Normalized near infrared spectra of the four RSGs in Westerlund 1, where the lines indicate the features studied. Green lines are for Ca II, blue lines indicate Fe I, black ones indicate the TiO molecular bandheads and the red line is for the VO bandhead.

mainly because of the general scarcity of RSGs.

In this work, using only the spectral range available ($\sim$ 8400 Å to $\sim$ 8900 Å), spectral types of the four RSGs in Westerlund 1 were determined by means of a visual and qualitative classification based on the strength of Ca II (CaT) and Fe I lines together with the depth of titanium oxide (TiO) and vanadium oxide (VO) molecular bands. Ca II and Fe I lines begin to weaken around the middle K types and continue to do so for later types, while TiO and VO molecular bands first appear at the M0 type and grow deeper with later types and descreasing temperatures (Levesque et al. 2005, Dorda et al. 2016), affecting the nearby continuum. These features were carefully compared among a set of stars with different spectral types, including the four RSGs of interest. A relation of all the reference stars used is given in table B.1 and a list of all the features that were compared is in tables B.2 and B.3. The results of the classification, according to the different epochs

and features analyzed, are presented in table 3.1 and 3.2.

	Features				SpT
Star	TiO	VO	CaT	Fe I	range
W237	M4/M5	M5/M6	M4/M5	M4/M5	M4-M6
W20	M3/M4	M5/M6	M3/M4	M4	M3-M6
W26	**M0.5/M1**	M3/M4	M3/M4	M3/M4	M3-M4
W75	M1	M1	M1	M1	M1

Table 3.1 - Spectral types of the four RSGs in Westerlund 1, in epoch 1.

	Features				SpT
Star	TiO	VO	CaT	Fe I	range
W237	M4/M5	M5/M6	M4/M5/M6	M5/M6	M4-M6
W20	M4/M5	M5/M6	M4/M5	M4/M5	M4-M6
W26	**M1**	M3/M4	M4/M5/M6	M4/M5	M3-M6

Table 3.2 - Spectral types of three of the RSGs in Westerlund 1, in epoch 2.

It can be seen that there is a slight spectral variability from epoch 1 to epoch 2 yielding variations of one spectral subtype in less than four years. As mentioned in section 1.2.5.2, this is expected and unsurprising for RSGs.

The difficulty of the classification varied within the features analyzed. In the case of the Fe I lines, for instance, every one of the fourteen lines that were compared among different stars suggested a slightly different, and sometimes a very different spectral type. On the other hand, comparing the VO molecular bands was fairly easy. However, all the features can come to an agreement with an uncertainty of about one subtype. This way, W20 can be classified as a type M4.5, with an uncertainty of ± 1.5 subtypes; W26 would be a type M4, with an uncertainty of ± 1 subtype; and W237 would be type M5, also with an uncertainty of ± 1 subtype. W75 is clearly a type M1 according to this classification, however, based on the low S/N of the only spectrum available, the uncertainty would probably be greater than ± 1 subtype.

Interestingly, according to the TiO bands at (8432 + 8442 + 8452) Å , W26 is type M1, which is quite an earlier subtype than the other features suggest. However, the band at 8859 Å in the spectrum obtained in epoch 2 looks sufficiently deep to correspond to a

spectral type later than M1. So for this star, a later type more consistent with the other features was assigned.

Although the spectra analyzed in this work do not present much variability between epochs 1 and 2, it is evident from previous works that it is difficult to classify the RSGs in Westerlund 1 due the spectral variations they show over a few years. For example, Clark et al. 2010 performed a classification of these four stars by using spectra obtained between years 2001 and 2006, that is consistent with the results of this work. They pose that W26 presents significant changes in spectral type that goes from M2 Ia to M5 Ia, and that W20 and W237 are type M5 Ia, while Mengel and Tacconi-Garman 2007 classify W237 as type M3 Ia. About W75, Clark et al. 2010 say that it presents a discrepancy between optical and NIR classifications, showing to be type M0 Ia in the first case and M4 Ia in the second.

3.2 Effective temperature determination by using Fe I lines

Spectra of the four RSGs were also used to estimate their effective temperatures. The results of this section will be compared to the ones obtained with the photometric analysis.

Since Fe I lines are produced in the photosphere, they can be associated to effective temperatures and in fact, Dorda et al. 2016 show that equivalent widths (EW) of Fe I lines strongly depend on T_{eff}, decreasing as the latter goes colder than than 4000 K (see figure 3.2).

This way, to estimate the temperature of the RSGs in Westerlund 1, the equivalent widths of the Fe I spectral lines listed in table B.2 were measured according to the line and continuum ranges indicated, and compared to the ones measured on spectra of the reference stars listed in B.1.

As an example, W20 is compared to some of the reference stars in figure 3.3: First, a graphic comparison of EWs is made, as shown in (a). Then, when it is determined which reference stars are the most similar to W20 in (b), linear fits are performed and the most appropriate one for a 1:1 relationship is chosen, in (c). The best linear fit will indicate the reference star which is analog, or most similar, to W20 in temperature and hence, the T_{eff} of the first will be assigned to the second. In this case, EWs measured for the stars HD 100930, HD 93420 and V396 Cen are closest to the ones measured for W20 both in epochs 1 and 2, but the best linear fit, that is the one closest to a 1:1 relationship, is given

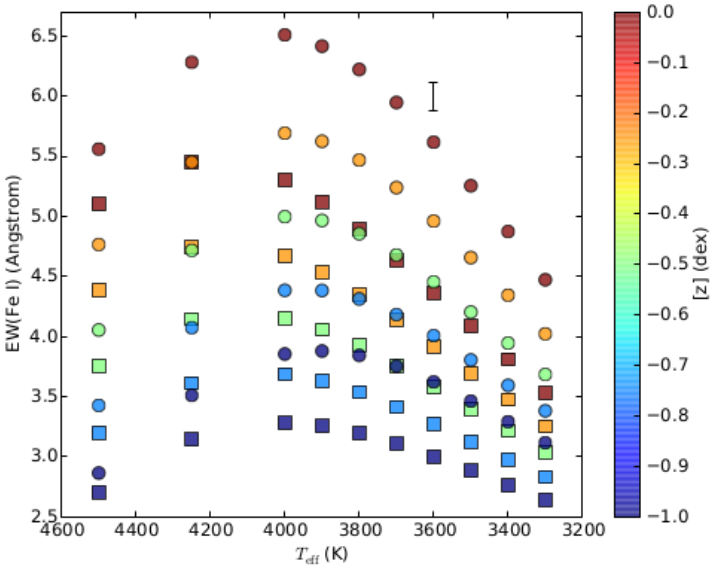

Figure 3.2: Image taken from Dorda et al. (2016) that shows the dependence of EWs of Fe I lines on T_{eff}. EWs were measured in synthetic spectra based on MARCS atmospheric models, for different metallicities that correspond to different colors, and for different surface gravities (circles for log g = 0.0 and squares for log g = 1.0).

by V396 Cen. So, W20 should have a temperature of (3550 ± 100) K, which is the T_{eff} of V396 Cen according to Levesque et al. 2005. It is worth noting that the T_{eff}'s of HD 100930 and HD 93420 are 3600 K and 3525 K respectively (also from Levesque et al. 2005), which fit within the error.

Following the same procedure for the other three stars, it is concluded that W26 has the same effective temperature as HD 339034 in epoch 1 and KW Sgr in epoch 2, W75 has the same T_{eff} as HD 339034 in epoch 1 (the only one available), and W237 has the same T_{eff} as V396 Cen in both epochs. The best linear fits obtained are summarized in table 3.3, and in table 3.4 the T_{eff}'s estimated by this method are summarized together with the analog reference stars and the literature giving their temperatures.

3.3 Luminosity determination and Hertzsprung-Russell diagram

In this section, just like in chapter 2, T_{eff} is used to calculate BC_K through equation 1.3. With it, M_{bol} is obtained and finally, luminosity is determined by the relation $M_{bol} = M_{bol_\odot} - 2.5log(L/L_\odot)$, where $M_{bol_\odot} = 4.74$. Also, the radius is obtained by means of the black body approximation of section 1.2.3.5. Results are summarized in table 3.5 and will

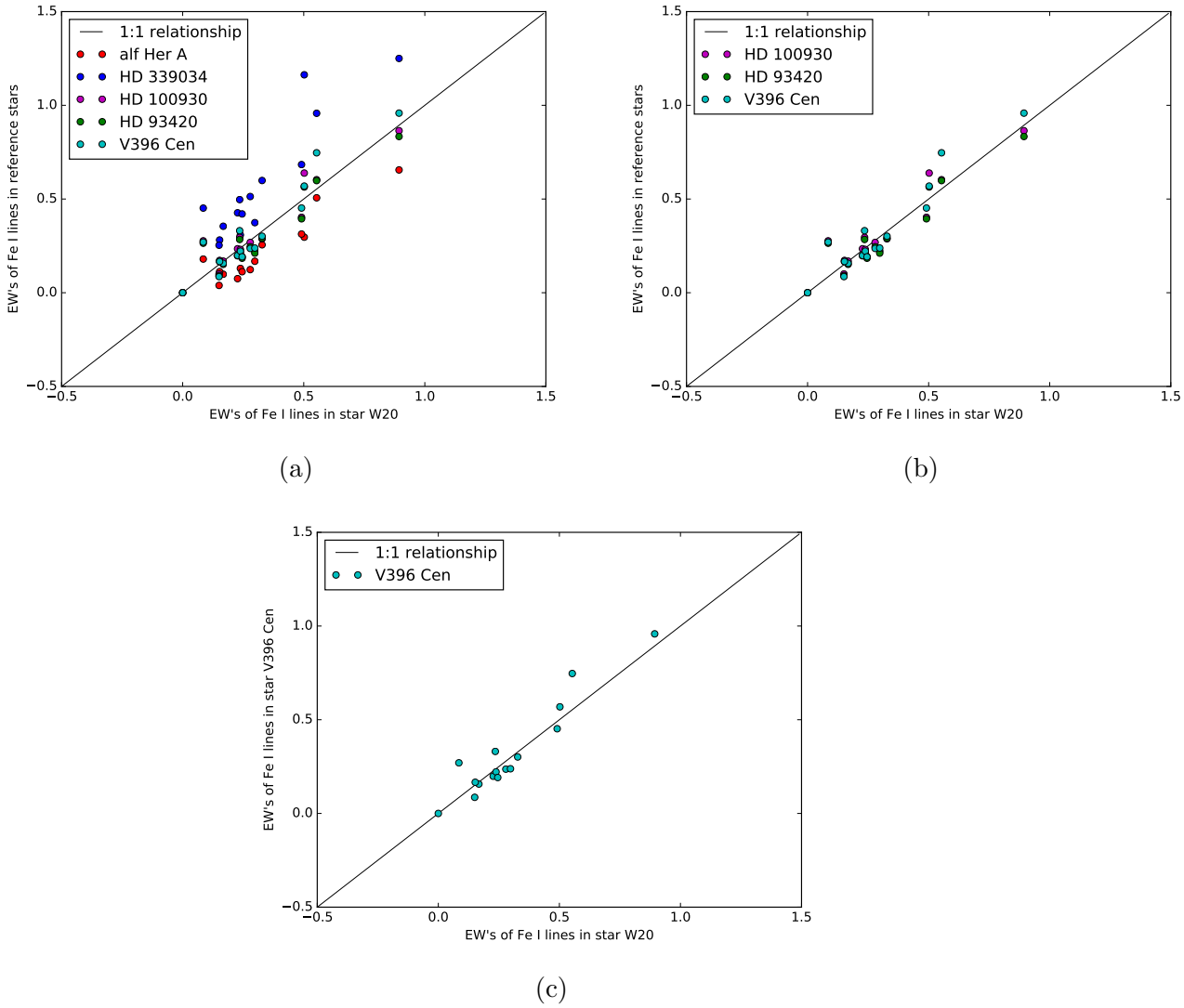

Figure 3.3: Figure (a) compares EWs of Fe I lines measured for W20 and some reference stars. Figure (b) shows the stars with most similar EWs to W20, and figure (c) shows the star closest to a 1:1 relationship (see text). EWs here were measured on spectra from epoch 1.

Star	Epoch of observation	Best 1:1 relationship	Slope	Intercept	R^2	Standard error
W20	1	V396 Cen	1.07	0.00	0.87	0.09
	2	V396 Cen	0.95	0.07	0.90	0.08
W26	1	HD 339034	1.03	0.05	0.95	0.07
	2	KW Sgr	0.98	-0.01	0.94	0.06
W75	1	HD 339034	1.06	0.01	0.87	0.12
	2	-	-	-	-	-
W237	1	V396 Cen	0.94	0.01	0.92	0.07
	2	V396 Cen	1.12	0.03	0.85	0.10

Table 3.3 - Linear fits for the best 1:1 relationships between the four RSGs in Westerlund 1 and the reference stars.

	Analog Star				
Star	epoch 1	epoch 2	T_{eff}(K)	ΔT_{eff}(K)	Reference
W237	V396 Cen	V396 Cen	3550	100	Levesque et al. 2005
W20	V396 Cen	V396 Cen	3550	100	Levesque et al. 2005
W26	HD 339034		4000	100	Levesque et al. 2005
		KW Sgr	3720	183	Arroyo-Torres et al. 2013
W75	HD 339034	-	4000	100	Levesque et al. 2005

Table 3.4 - Effective temperatures derived from the equivalent widths of Fe I spectral lines.

be added to the Hertzsprung-Russell diagram presented in section 2.5.

Star	T_{eff}(K)	BC_K	M_{bol}	$L(\times 10^5 L_\odot)$	$R(R_\odot)$
W237	3550 ± 100	2.88 ± 0.08	-8.61 ± 0.13	2.19 ± 0.26	1241 ± 70
W20	3550 ± 100	2.88 ± 0.08	-7.81 ± 0.13	1.05 ± 0.13	858 ± 48
W26	4000 ± 100	2.54 ± 0.08	-8.99 ± 0.13	3.12 ± 0.37	1165 ± 58
	3720 ± 183	2.75 ± 0.14	-8.78 ± 0.17	2.56 ± 0.40	1221 ± 120
W75	4000 ± 100	2.54 ± 0.08	-7.95 ± 0.13	1.20 ± 0.14	722 ± 36

Table 3.5 - Calculations obtained from the effective temperatures derived from a spectral analysis of the four RSGs in Westerlund 1.

These results, derived from the spectral analysis, are shown in a new Hertzsprung-Russell diagram in figure 3.4 together with the ones obtained in chapter 2, but this time omitting the points corresponding to stars W20 and W75 that in figure 2.3 are far to the right of the evolutionary tracks, and therefore are unreliable.

The first thing to mention about figure 3.4 is that, unlike with photometric data, by using their spectra it was possible to obtain reasonable points for W20 and W75, which show that both stars are a lot less luminous than the other RSGs.

It can be seen that the points are grouped according to the methods used to find their stellar parameters: To the left are the points, which T_{eff}'s and BC_K's were calculated from $(J-K)_0$ (blue and magenta), and to the right the ones calculated from $(V-K)_0$ (cyan and green). At a first glance, it would mean that points obtained from $(J-K)_0$ are more reliable, since they are closer to the evolutionary tracks, that is, they fit better to the models. Besides, it is expected to have better results from this color than from $(V-K)_0$, given the variability of RSGs in the V band.

On the other hand, black and red points correspond to temperatures obtained from the grid and the BC_K's of the red ones ultimately depend on the V magnitude because they were calculated directly from the BC_V's given by the grid. So, it makes sense that these points are in the same group of the ones obtained from $(V-K)_0$, and this indeed happens in the case of W26. However, it is not true for W237, which would mean that the grid is effectively not complete for cool stars, as warned by Worthey and Lee 2011.

About the yellow points obtained through the spectral analysis, they have to be obser-

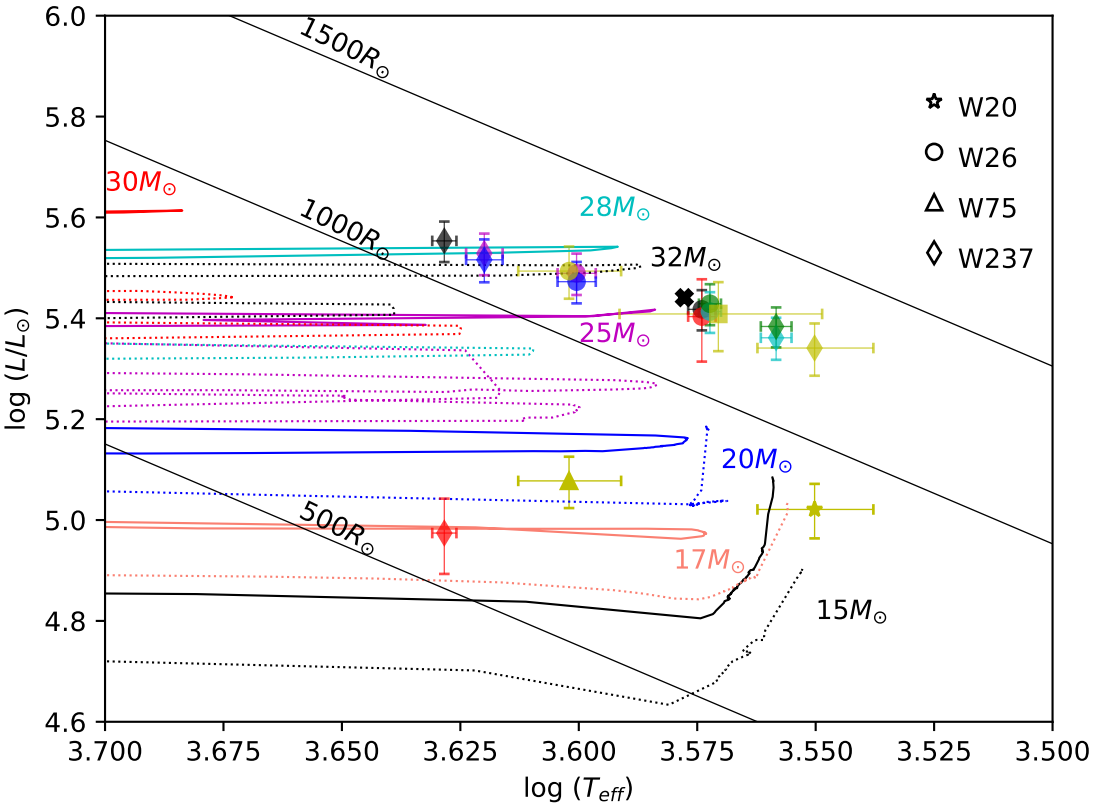

Figure 3.4: Luminosity vs. T_{eff} diagram in *log* units with evolutionary tracks from Ekström et al. 2012. The color and symbols are the same as in figure 2.3. The new points added in yellow are the ones obtained from the spectral analysis. The yellow square corresponds to the temperature estimated for W26 in epoch 2, while the circle corresponds to epoch 1. The black cross is the average point for W26.

ved star by star. W26 has two points, one in each of the groups mentioned before -one per epoch of observation-, that should be reliable due to the good S/N of the spectra obtained for this star. This, added to the fact that all eight points are not so spread out, allows to consider a weighted average value that was drawn in the HRD as a cross corresponding to the pair $T_{eff} = (3782 \pm 14)K$ and $L = (2.76 \pm 0.10) \times 10^5 L_\odot$. Fok et al. 2012 determined a similar temperature of 3700 K, but assuming a distance to the cluster of 3.5 kpc they derived a very different luminosity: $L = 1.1 \times 10^6 L_\odot$. On the other hand, Mackey et al. 2015 reports a temperature of $(3600 \pm 200)K$ obtained from model fitting, and Wright et al. 2014 reports that $L = 3.8 \times 10^5 L_\odot$ or $L = 3.2 \times 10^5 L_\odot$.

For W237 all seven points are more spread out, with the ones related to the V magnitude displaced to the right, far from the evolutionary tracks. For this reason, from now on only

the points obtained from $(J-K)_0$ will be considered, so for this star the following values are chosen to be the most reliable: An average luminosity of $L = (3.33 \pm 0.23) \times 10^5 L_\odot$ and $T_{eff} = (4168 \pm 37) K$, which differ from the ones reported by Fok et al. 2012: $T_{eff} = 3600K$ and $L = 2.3 \times 10^5 L_\odot$.

In the case of W20 and W75, yellow points are actually the only ones available (see table 3.5). Fok et al. 2012 also report similar values for W20: $T_{eff} = 3500K$ and $L = 1.3 \times 10^5 L_\odot$, but for W75 they report the values: $T_{eff} = 3600K$ and $L = 6.8 \times 10^5 L_\odot$, which disagree substantially with the ones obtained in this work. In fact, Fok et al. 2012 are the only authors that have derived effective temperatures and luminosities for all the four RSGs in Westerlund 1, however it is important to note that, as mentioned before, they assumed a distance to the cluster of 3.5 kpc, while here, a distance of 4.35 kpc is used.

Given all the above, the location of the cross would indicate that W26 has a mass of $25 M_\odot$ with rotation, or of $32 M_\odot$ without rotation. W237 would have a mass of $28 M_\odot$ with rotation, or of $32 M_\odot$ without rotation. W75 would have a $20 M_\odot$ mass and is probably non-rotating. Finally, W20 is closest to the $17 M_\odot$ no-rotation model or the $15 M_\odot$ rotational one.

3.4 Age of the RSGs in Westerlund 1

The age of the RSGs of interest in this work is determined with the help of the isochrone models of the Geneva grids of stellar evolution models (Ekström et al. 2012). A Hertzsprung-Russell diagram with isochrones is presented in figure 3.5, where it is shown that W26 and W237 fit better to the rotating model with age 7.9 Myr. The same age works well also for W75, but using the non-rotating model. W20 has a discrepant age with the rotating model (15.8 Myr) and even with the non-rotating one (10 Myr). Estimatives of mass (see section 3.3) and age are summarized in table 3.6.

It should be noted that three of the four RSGs appear to have the same age of 7.9 Myr, being W20 the only one older, but with a larger uncertainty. This way, a $t \sim 8 Myr$ could be adopted as the approximate age of the RSGs.

Interestingly, the RSGs in Westerlund 1 are about twice as old as the remaining of the cluster. This raises a lot of questions regarding the formation history of Westerlund 1 that are worth a broad research and analysis. However, this goes far beyong the objective

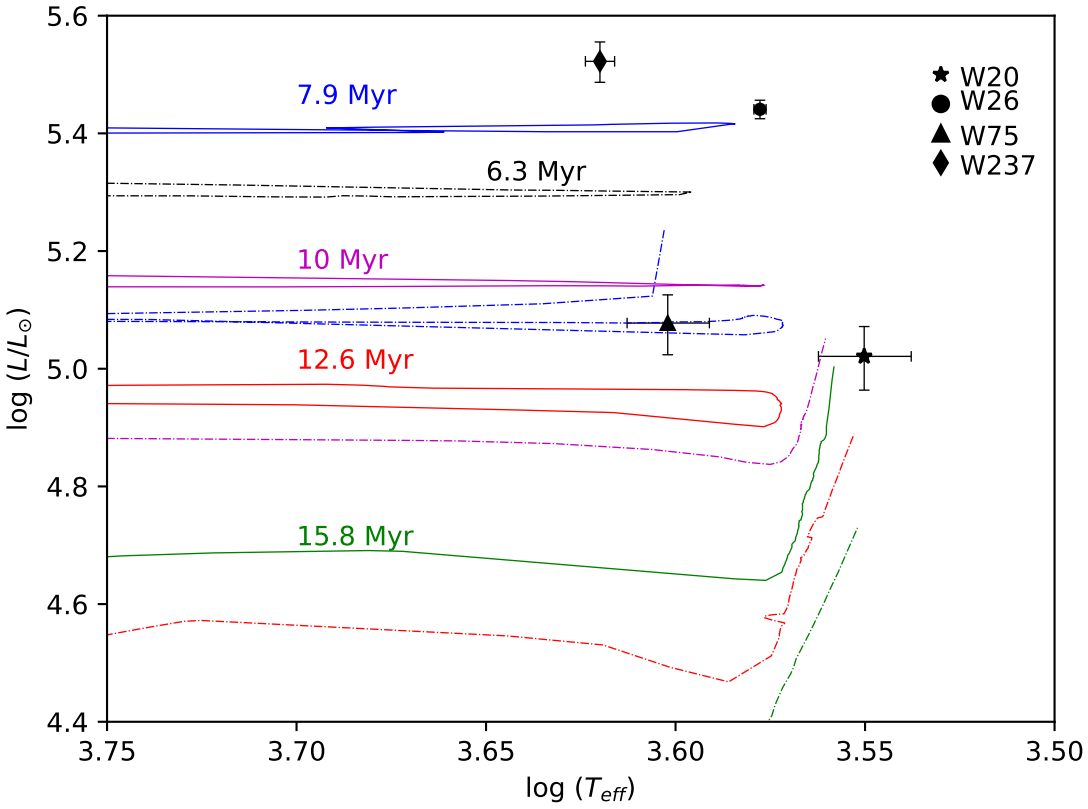

Figure 3.5: Luminosity vs. T_{eff} diagram in *log* units with isochrones from Ekström et al. 2012. Symbols correspond to stars as indicated, and colors link ages to their respective isochrones. Dotted lines are the no-rotation models and solid lines are the models with rotation.

	Mass ($M_\odot$)		Age (Myr)	
Star	rotating	non-rotating	rotating	non-rotating
W237	28	32	7.9	-
W20	15	17	15.8	10
W26	25	32	7.9	-
W75	-	20	-	7.9

Table 3.6 - Estimatives of mass and age for the RSGs in Westerlund 1.

of this dissertation, so the discussion that follows only aims at presenting briefly some possible reasons to this age difference and the problems that arise.

Red supergiants are expected to start appering after $\sim$ 7 Myr, however, and in spite of the multiple authors that have placed the age of Westerlund 1 around $\sim$ 4 Myr, none of

them have actually tried to solve this age paradox, where the membership of the stars to the cluster is key. Clark et al. 2005 argue that W20, W26 and W237 belong to the cluster based on their radio properties, which would result from membership to the cluster, and their comparable optical and mid-IR fluxes (in fact, Gennaro et al. 2017 used the $J - K$ color to separate the members of the cluster from fore- and background contamination). Also, Damineli et al. 2016 establish the membership of the RSGs by means of the interstellar extinction law in the direction of the cluster (see section 3.5). On the other hand, Lim et al. 2013 discuss the age problem more broadly and poses the doubt of whether or not the RSGs belong to the cluster and if they do, whether or not the population of the cluster is coeval. If it is not coeval, age and membership of the RSGs might not be incompatible. However, Kudryavtseva et al. 2012 had already given compelling arguments for Westerlund 1 to have formed in a nearly instantaneous starburst, with an age spread among cluster members constrained to 0.4 Myr. Besides, there is no evidence of bimodal formation, which also occurs in globular clusters such as 30 Doradus (see Cignoni et al. 2015), and would require an age spread greater than 0.5 Myr.

Under the assumption that the four RSGs are members of Westerlund 1, there is an interesting option to explain the age paradox: inflated envelopes. The central idea is that massive stars that approach the Eddington luminosity might present inflated evelopes with very low densities, however, this is not exactly the case as Sanyal et al. 2015 found that stars hardly ever reach the Eddington limit at their surface. For this reason, they considered an Eddington factor inside the star, defined as the ratio between the luminosity and Eddington luminosity, and actually showed that all stars above a certain mass will have this factor approaching to 1, that is they reach, and even exceed the Eddington limit *inside* the star producing the inflation of envelopes. Their models also show that inflation can produce core hydrogen burning red supergiants, that is, inflated stars that are still in the main sequence and resemble older RSGs. This could explain why a young cluster such as Westerlund 1 has stars that appear to double its age. This hypothesis would at least fit to W26 and W237, since Sanyal et al. 2017 studied the metallicity dependence of envelope inflation and showed that massive stars in the Milky Way present inflation above $\sim 29 M_{\odot}$.

Another solution to the age paradox could imply the miscalculation of the cluster's age. By fitting main sequence (MS) stars in a color-magnitude diagram, Naylor 2009 derived ages for young clusters and associations that are a factor of 1.5 or 2 longer than the ages

derived from fitting isochrones to pre-main sequence stars (PMS, see figure 3.6), which is how cluster ages are usually determined and how in fact, the age of Westerlund 1 was determined by Brandner et al. 2008 and Gennaro et al. 2011. Therefore, the actual age of the cluster would be about the same of the RSGs, as indicated by the red point that was added to figure 3.6.

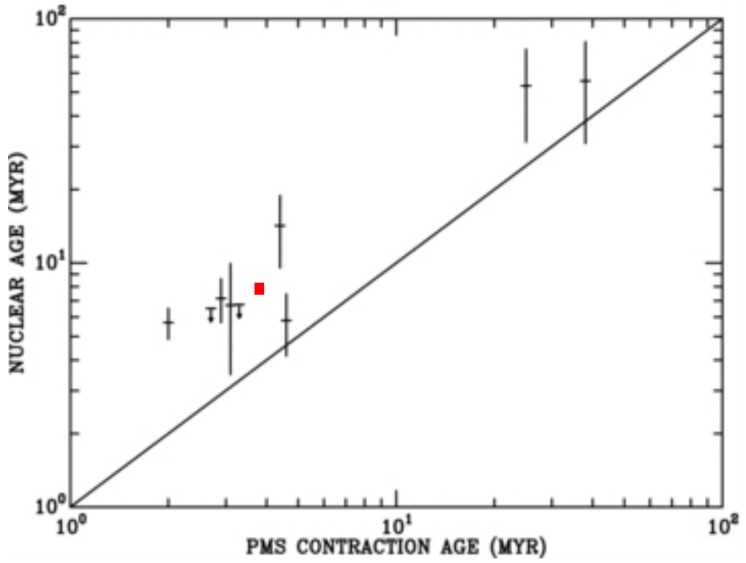

Figure 3.6: This is Figure 9 in the paper by Naylor 2009 that shows the difference between ages determined from the Main Sequence (nuclear age) and the Pre-Main Sequence. MS ages are a factor of 2 larger, on average. The red point was added here to indicate the ages for Westerlund 1 derived from the PMS ($\sim 3.8 Myr$) and the RSGs ($\sim 8 Myr$).

3.5 Gaia DR2

In addition to the membership of the four RSGs to Westerlund 1, evaluating the distance, not only to the cluster, but also to the stars is crucial. In chapter 2, the distance to the cluster (4.35 kpc) was used to calculate the absolute magnitudes of the stars. However, individual distances to the RSGs would obviously improve those calculations and the Gaia mission could help, although it seems that the cluster is too far away for its capability. In fact, the Gaia Data Release 2 (April 25, 2018) still does not provide reliable parallaxes for the stars in Westerlund 1, including the four RSGs. As seen in table 3.7, this release gives distances ranging from 0.6 to 7 Kpc for the stars in the cluster. The errors are gaussian and would change if a bayesian approach was adopted, but the approximate distances would remain the same.

Members						
Star	EW 8620 (Å)	A_K	Parallax	Paral. error	Dist. (kpc)	Dist. error (kpc)
W237	0.81	0.74	1.64	0.26	0.61	0.10
W32	0.87	0.73	1.23	0.17	0.81	0.11
W12a	0.87	0.81	1.06	0.17	0.94	0.15
W243	0.98	0.7	0.98	0.16	1.02	0.17
W4	0.85	0.66	0.97	0.14	1.03	0.15
W265	0.89	0.79	0.80	0.17	1.25	0.26
W8a	0.85	0.68	0.72	0.17	1.40	0.34
W26	0.88	0.73	0.68	0.25	1.47	0.53
W16a	0.78	0.75	0.58	0.17	1.72	0.51
W7	0.83	0.77	0.48	0.16	2.06	0.68
W70	0.85	0.75	0.43	0.15	2.34	0.80
W20	0.84	0.96	0.26	0.26	3.84	3.80
W2a	0.89	0.67	0.19	0.12	5.27	3.38
W75	-	-	0.14	0.22	6.98	10.96
W71	1.04	0.77	-0.09	0.14	-11.62	18.35
Non-members						
HD 151018	0.18	0.25	0.48	0.05	2.10	0.20

Table 3.7 - Extinction indicators and distances from the Gaia DR2, for members of Westerlund 1 and the foreground star HD 151018.

Figure 3.7, adapted from Damineli et al. 2016, allows to confirm that the distances provided by Gaia DR2 are unreliable for this cluster. It shows that insterstellar extinction is well behaved for all cluster members when using the extinction A_K or the equivalent width of the 8620 Å diffuse interstellar band (DIB). All the cluster members in the figure have a large extinction and are packed around average values for the extinction indicators: EW 8620 Å $= 0.92 \pm 0.08$, and $A_K = 0.73 \pm 0.06$, indicating that the distances should not be so different. However, Gaia DR2 provides distances with a large spread between the 14 cluster members, indicating that they are unreliable. It also can be seen that the star HD 151018 is a bright foreground to the cluster to which Gaia DR2 gives a distance of 2.1 $\pm$ 0.2 kpc, while distances for the stars in Westerlund 1 are even smaller than that. Given that the extinction indicators of HD 151018 are about 1/5 of the ones for Westerlund 1, the distance to this foreground star should also be $\sim 1/5$ of the distance to the cluster. That is to say that for distances to members of the cluster, the Gaia DR2 presents systematic errors that are much bigger than the statistical ones. Moreover, for W20 and W75, the statistical errors are overly big.

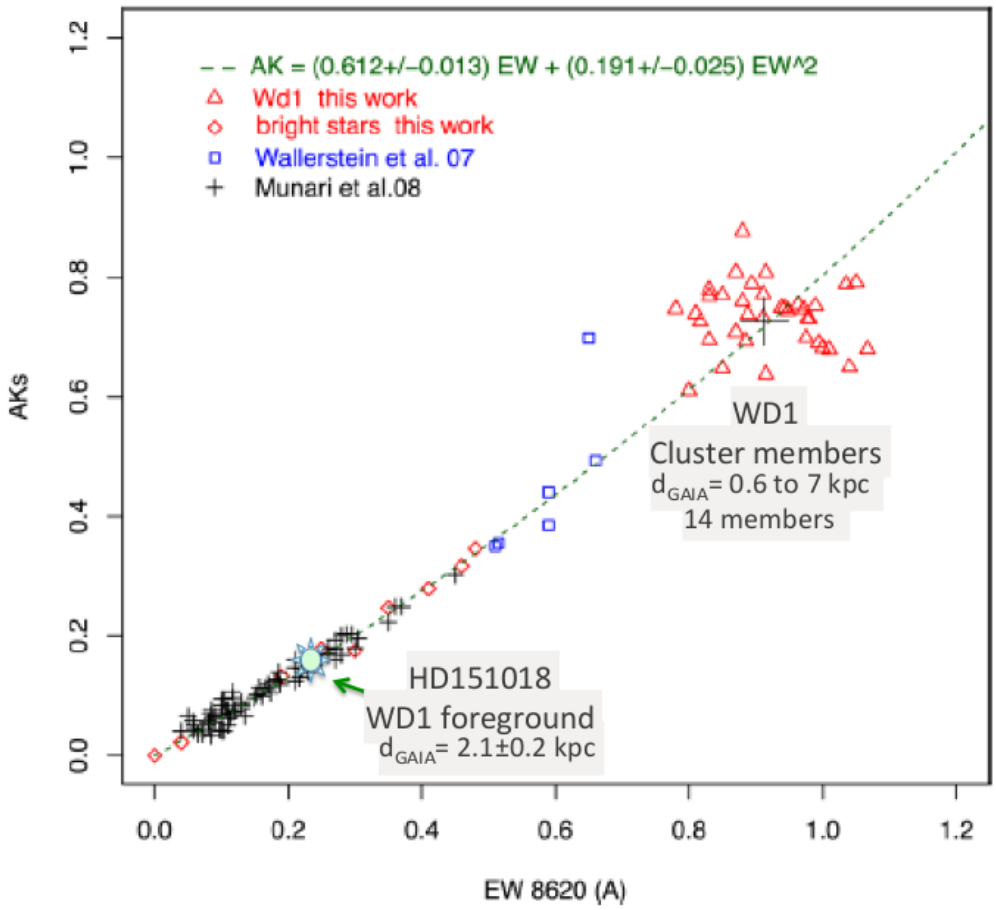

Figure 3.7: Insterstellar extinction law in the direction of Westerlund 1, showing the low extinction of the foreground star HD 151018. Adapted from Damineli et al. 2016.

Chapter 4

Conclusions and Perspectives

By using JHK band photometry, effective temperatures and luminosities of the four RSGs in Westerlund 1 were determined by different methods, which showed to be particularly consistent in the case of W26. Results obtained for W26 and W237 favored the methods that involved the color $(J-K)_0$, since they agree better with the evolutionary tracks. The photometric analysis did not provide good results for W20 and W75, but showed that these stars have an excess of emission at the K band related to the presence of hot dust.

Spectra obtained in two different epochs for W20, W26 and W237, and in only one epoch for W75 were visually compared to spectra of well known reference stars, in order to perform a spectral type classification. This comparison was made based on the depth of TiO and VO molecular bands and the strength of CaT and Fe I atomic lines in the range from 8400 Å to 8900 Å. Spectral types were assigned as follows, with uncertainties of ± 1 subtype: W20 = M4.5 I, W26 = M4 I, W237 = M5 I and W75 = M1 I.

Given their strong dependence on T_{eff}, equivalent widths of Fe I atomic lines were measured in all the spectra. Then, the ones obtained from spectra of the four RSGs were compared to the ones from spectra of the reference stars, looking for the best 1:1 relationship. This way, new effective temperatures were assigned to the RSGs and from them, luminosities were calculated again. The spectral analysis provided results similar to the ones obtained from the photometric analysis, and in the case of W20 and W75, provided the only reliable ones.

With the stars already located in the HRD, evolutionary tracks and isochrones were superimposed so that initial masses and ages could be determined. With an average age of 8 Myr, the four RSGs are about twice as old as Westerlund 1, leading to uncertainties

still unresolved about the formation history of the cluster. Some possible solutions to this paradox were discussed. The hypotheses of inflated envelopes and the apparently poorly constrained age of young clusters like Westerlund 1, by means of the PMS fitting, need further examination.

To better constrain the stellar parameters of the four RSGs, high resolution spectroscopy at JHK bands together with 3D modeling is necessary. Fitting the spectral energy distributions (SEDs) to synthetic spectra would allow a more precise determination of effective temperatures and consequently, of luminosities. Also, distances in future Gaia data releases need to be considered to improve the calculations.

Bibliography

Almeida L., Damineli A., Distance to Westerlund 1 using eclipsing binaries, 2018, in preparation.

Arroyo-Torres B., Wittkowski M., Marcaide J. M., Hauschildt P. H., The atmospheric structure and fundamental parameters of the red supergiants AH Scorpii, UY Scuti, and KW Sagittarii, A&A, 2013, vol. 554, p. A76

Bessell M. S., Wood P. R., A note on bolometric corrections for late-type stars and long-period variables, PASP, 1984, vol. 96, p. 247

Brandner W., Clark J. S., Stolte A., Waters R., Negueruela I., Goodwin S. P., Intermediate to low-mass stellar content of Westerlund 1, A&A, 2008, vol. 478, p. 137

Britavskiy N. E., Bonanos A. Z., Mehner A., García-Álvarez D., Prieto J. L., Morrell N. I., Identification of red supergiants in nearby galaxies with mid-IR photometry, A&A, 2014, vol. 562, p. A75

Carquillat M. J., Jaschek C., Jaschek M., Ginestet N., An Atlas of the infrared spectral region. II. The late-type stars (G - M), A&AS, 1997, vol. 123, p. 5

Chiavassa A., Freytag B., Masseron T., Plez B., Radiative hydrodynamics simulations of red supergiant stars. IV. Gray versus non-gray opacities, A&A, 2011, vol. 535, p. A22

Chiavassa A., Haubois X., Young J. S., Plez B., Josselin E., Perrin G., Freytag B., Radiative hydrodynamics simulations of red supergiant stars. II. Simulations of convection on Betelgeuse match interferometric observations, A&A, 2010, vol. 515, p. A12

Chiavassa A., Plez B., Josselin E., Freytag B., Radiative hydrodynamics simulations of red supergiant stars. I. interpretation of interferometric observations, A&A, 2009, vol. 506, p. 1351

Cignoni M., Sabbi E., van der Marel R. P., Tosi M., Zaritsky D., Anderson J., Lennon D. J., Aloisi A., de Marchi G., Gouliermis D. A., Grebel E. K., Smith L. J., Zeidler P., Hubble Tarantula Treasury Project. II. The Star-formation History of the Starburst Region NGC 2070 in 30 Doradus, ApJ, 2015, vol. 811, p. 76

Clark J. S., Negueruela I., Crowther P. A., Goodwin S. P., On the massive stellar population of the super star cluster Westerlund 1, A&A, 2005, vol. 434, p. 949

Clark J. S., Negueruela I., Davies B., Larionov V. M., Ritchie B. W., Figer D. F., Messineo M., Crowther P. A., Arkharov A. A., A third red supergiant rich cluster in the Scutum-Crux arm, A&A, 2009, vol. 498, p. 109

Clark J. S., Ritchie B. W., Najarro F., Langer N., Negueruela I., A VLT/FLAMES survey for massive binaries in Westerlund 1. IV. Wd1-5 - binary product and a pre-supernova companion for the magnetar CXOU J1647-45?, A&A, 2014, vol. 565, p. A90

Clark J. S., Ritchie B. W., Negueruela I., A serendipitous survey for variability amongst the massive stellar population of Westerlund 1, A&A, 2010, vol. 514, p. A87

Clark S., Negueruela I., Ritchie B., Najarro P., Langer N., Crowther P., Bartlett L., Fenech D., González-Fernández C., Goodwin S., Lohr M., Prinja R., An Astrophysical Laboratory: Understanding and Exploiting the Young Massive Cluster Westerlund 1, The Messenger, 2015, vol. 159, p. 30

Crowther P. A., Hadfield L. J., Clark J. S., Negueruela I., Vacca W. D., A census of the Wolf-Rayet content in Westerlund 1 from near-infrared imaging and spectroscopy, MNRAS, 2006, vol. 372, p. 1407

Damineli A., Almeida L. A., Blum R. D., Damineli D. S. C., Navarete F., Rubinho M. S., Teodoro M., Extinction law in the range 0.4-4.8 μm and the 8620 Å DIB towards the stellar cluster Westerlund 1, MNRAS, 2016, vol. 463, p. 2653

Dorda R., González-Fernández C., Negueruela I., Characterisation of red supergiants in the Gaia spectral range, A&A, 2016, vol. 595, p. A105

Dorda R., Negueruela I., González-Fernández C., Tabernero H. M., Spectral type, temperature, and evolutionary stage in cool supergiants, A&A, 2016, vol. 592, p. A16

Drout M. R., Massey P., Meynet G., The Yellow and Red Supergiants of M33, ApJ, 2012, vol. 750, p. 97

Ekström S., Georgy C., Eggenberger P., Meynet G., Mowlavi N., Wyttenbach A., Granada A., Decressin T., Hirschi R., Frischknecht U., Charbonnel C., Maeder A., Grids of stellar models with rotation. I. Models from 0.8 to 120 $M_{\odot}$ at solar metallicity (Z = 0.014), A&A, 2012, vol. 537, p. A146

Elias J. H., Frogel J. A., Humphreys R. M., M supergiants in the Milky Way and the Magellanic Clouds Colors, spectral types, and luminosities, ApJS, 1985, vol. 57, p. 91

Fok T. K. T., Nakashima J.-i., Yung B. H. K., Hsia C.-H., Deguchi S., Maser Observations of Westerlund 1 and Comprehensive Considerations on Maser Properties of Red Supergiants Associated with Massive Clusters, ApJ, 2012, vol. 760, p. 65

Gehrz R., Sources of Stardust in the Galaxy. In Interstellar Dust , vol. 135 of IAU Symposium, 1989, p. 445

Gennaro M., Brandner W., Stolte A., Henning T., Mass segregation and elongation of the starburst cluster Westerlund 1, MNRAS, 2011, vol. 412, p. 2469

Gennaro M., Goodwin S. P., Parker R. J., Allison R. J., Brandner W., Hierarchical formation of Westerlund 1: a collapsing cluster with no primordial mass segregation?, MNRAS, 2017, vol. 472, p. 1760

Ginestet N., Carquillat J. M., Jaschek M., Jaschek C., Spectral classifications in the near infrared of stars with composite spectra. I. The study of MK standards., A&AS, 1994, vol. 108, p. 359

González-Fernández C., Dorda R., Negueruela I., Marco A., A new survey of cool supergiants in the Magellanic Clouds, A&A, 2015, vol. 578, p. A3

Houdashelt M. L., Bell R. A., Sweigart A. V., Improved Color-Temperature Relations and Bolometric Corrections for Cool Stars, AJ, 2000, vol. 119, p. 1448

Humphreys R. M., McElroy D. B., The initial mass function for massive stars in the Galaxy and the Magellanic Clouds, ApJ, 1984, vol. 284, p. 565

Kirkpatrick J. D., Henry T. J., McCarthy Jr. D. W., A standard stellar spectral sequence in the red/near-infrared - Classes K5 to M9, ApJS, 1991, vol. 77, p. 417

Kudryavtseva N., Brandner W., Gennaro M., Rochau B., Stolte A., Andersen M., Da Rio N., Henning T., Tognelli E., Hogg D., Clark S., Waters R., Instantaneous Starburst of the Massive Clusters Westerlund 1 and NGC 3603 YC, ApJ, 2012, vol. 750, p. L44

Kupka F. G., Ryabchikova T. A., Piskunov N. E., Stempels H. C., Weiss W. W., VALD-2 – The New Vienna Atomic Line Database, Baltic Astronomy, 2000, vol. 9, p. 590

Levesque E. M., Astrophysics of Red Supergiants. 2514-3433, IOP Publishing, 2017

Levesque E. M., Massey P., Spectral Types of Red Supergiants in NGC 6822 and the Wolf-Lundmark-Melotte Galaxy, AJ, 2012, vol. 144, p. 2

Levesque E. M., Massey P., Olsen K. A. G., Plez B., Late-Type Red Supergiants: Too Cool for the Magellanic Clouds?, ApJ, 2007, vol. 667, p. 202

Levesque E. M., Massey P., Olsen K. A. G., Plez B., Josselin E., Maeder A., Meynet G., The Effective Temperature Scale of Galactic Red Supergiants: Cool, but Not As Cool As We Thought, ApJ, 2005, vol. 628, p. 973

Levesque E. M., Massey P., Olsen K. A. G., Plez B., Meynet G., Maeder A., The Effective Temperatures and Physical Properties of Magellanic Cloud Red Supergiants: The Effects of Metallicity, ApJ, 2006, vol. 645, p. 1102

Lim B., Chun M.-Y., Sung H., Park B.-G., Lee J.-J., Sohn S. T., Hur H., Bessell M. S., The Starburst Cluster Westerlund 1: The Initial Mass Function and Mass Segregation, AJ, 2013, vol. 145, p. 46

Mackey J., Castro N., Fossati L., Langer N., Cold gas in hot star clusters: the wind from the red supergiant W26 in Westerlund 1, A&A, 2015, vol. 582, p. A24

Maeder A., Lequeux J., Azzopardi M., The numbers of red supergiants and WR stars in galaxies - an extremely sensitive indicator of chemical composition, A&A, 1980, vol. 90, p. L17

Massey P., Evolved Massive Stars in the Local Group. I. Identification of Red Supergiants in NGC 6822, M31, and M33, ApJ, 1998, vol. 501, p. 153

Massey P., A UBVR CCD Survey of the Magellanic Clouds, ApJS, 2002, vol. 141, p. 81

Massey P., Levesque E. M., Olsen K. A. G., Plez B., Skiff B. A., HV 11423: The Coolest Supergiant in the SMC, ApJ, 2007, vol. 660, p. 301

Massey P., Olsen K. A. G., The Evolution of Massive Stars. I. Red Supergiants in the Magellanic Clouds, AJ, 2003, vol. 126, p. 2867

Massey P., Silva D. R., Levesque E. M., Plez B., Olsen K. A. G., Clayton G. C., Meynet G., Maeder A., Red Supergiants in the Andromeda Galaxy (M31), ApJ, 2009, vol. 703, p. 420

Mengel S., Tacconi-Garman L. E., Medium resolution 2.3 μm spectroscopy of the massive Galactic open cluster Westerlund 1, A&A, 2007, vol. 466, p. 151

Naylor T., Are pre-main-sequence stars older than we thought?, MNRAS, 2009, vol. 399, p. 432

Negueruela I., Massive Young Stellar Clusters in the Milky Way, Highlights of Spanish Astrophysics V, 2010, vol. 5, p. 171.

Negueruela I., Clark J. S., Ritchie B. W., The population of OB supergiants in the starburst cluster Westerlund 1, A&A, 2010, vol. 516, p. A78

Sanyal D., Grassitelli L., Langer N., Bestenlehner J. M., Massive main-sequence stars evolving at the Eddington limit, A&A, 2015, vol. 580, p. A20

Sanyal D., Langer N., Szécsi D., -C Yoon S., Grassitelli L., Metallicity dependence of envelope inflation in massive stars, A&A, 2017, vol. 597, p. A71

Smartt S. J., Observational Constraints on the Progenitors of Core-Collapse Supernovae: The Case for Missing High-Mass Stars, PASA, 2015, vol. 32, p. e016

Solf J., Spectral type and luminosity classification of late-type M stars from near-infrared image tube coudé spectrograms., A&AS, 1978, vol. 34, p. 409

Stothers R. B., Giant Convection Cell Turnover as an Explanation of the Long Secondary Periods in Semiregular Red Variable Stars, ApJ, 2010, vol. 725, p. 1170

Ulmer A., Fitzpatrick E. L., Revisiting the Modified Eddington Limit for Massive Stars, ApJ, 1998, vol. 504, p. 200

Valenti J. A., Piskunov N., Johns-Krull C. M., Spectral Synthesis of TiO Lines, ApJ, 1998, vol. 498, p. 851

van Loon J. T., Observed properties of red supergiant and massive AGB star populations, Mem. Soc. Astron. Italiana, 2017, vol. 88, p. 354

VandenBerg D. A., Clem J. L., Empirically Constrained Color-Temperature Relations. I. BV(RI)$_C$, AJ, 2003, vol. 126, p. 778

Wenger M., Ochsenbein F., Egret D., Dubois P., Bonnarel F., Borde S., Genova F., Jasniewicz G., Laloë S., Lesteven S., Monier R., The SIMBAD astronomical database. The CDS reference database for astronomical objects, A&AS, 2000, vol. 143, p. 9

Worthey G., Lee H.-c., An Empirical UBV RI JHK Color-Temperature Calibration for Stars, ApJS, 2011, vol. 193, p. 1

Wright N. J., Wesson R., Drew J. E., Barentsen G., Barlow M. J., Walsh J. R., Zijlstra A., Drake J. J., Eislöffel J., Farnhill H. J., The ionized nebula surrounding the red supergiant W26 in Westerlund 1, MNRAS, 2014, vol. 437, p. L1

Appendix

Appendix A

Observational Data

A.1 Spectroscopic Data

Details about the spectra used in this work are summarized in table A.1.

Object	Date of observation	Telescope	Spectrograph	Grating	Slit
W237	July 5, 2012	1.6 m (OPD)	Coudé	-	-
	July 4, 2017	SOAR	Goodman	930 l/mm	0.46" long slit
W20	July 18, 2013	1.6 m (OPD)	Coudé	-	-
	July 4, 2017	SOAR	Goodman	930 l/mm	0.46" long slit
W26	July 5, 2012	1.6 m (OPD)	Coudé	-	-
	July 4, 2017	SOAR	Goodman	930 l/mm	0.46" long slit
W75	August 7, 2014	1.6 m (OPD)	Coudé	-	-

Table A.1 - Details of the spectroscopic data used.

Appendix B

Lists of Reference Stars and Spectral Features Measured

B.1 Reference stars

Name	Type	Description
alf Her A	M5Ib	Long-period variable
alf Sco	M1.5Iab	Red supergiant
HD 93420	M4Ib	Long-period variable
HD 207076	M7-III	Asymptotic Giant Branch
HD 339034	M1Ia	Red supergiant
HD 100930	M2.5Iab-Ib	Red supergiant
HD 113285	M8III	Asymptotic Giant Branch
HD 126327	M7.5-M8	Asymptotic Giant Branch
HIP 74995	M3V	Variable of BT Dra type
HIP 85658	M3(III)	-
HIP 92783	M0/1	-
KW Sgr	M4Ia - M1.5 I*	Red supergiant
UY Sct	M4Ia	Red supergiant
V396 Cen	M4Ia-Iab	Red supergiant

Table B.1 - Reference stars used to compare to the the RSGs in Westerlund 1. Spectral types and descriptions are taken from the SIMBAD Astronomical Database (Wenger et al. 2000).
* Levesque et al. (2005) classified KW Sgr as M1.5 I.

B.2 Features measured

Atomic Lines		Range of EW measurement (Å)		Pseudocontinuum ranges (Å)		
Wavelength (Å)	Chemical species	Lower limit	Upper limit	At Blue	At Red	Reference
8498.0	Ca II	8492.5	5803.5	8492.2-8490.4	8507.6-8509.6	Solf (1978)
8514.1	Fe I	8512.5	8516.3	8507.6-8509.6	8557.5-8559.0	Carquillat et al. (1997)
8542.0	Ca II	8532.0	8553.0	8507.6-8509.6	8557.5-8559.0	Solf (1978)
8582.0	Fe I	8581.0	8583.7	8579.5-8580.8	8600.0-8602.0	Carquillat et al. (1997)
8611.0	Fe I	8610.9	8612.7	8600.0-8602.2	8619.6-8620.6	Carquillat et al. (1997)
8621.5	Fe I	8620.6	8622.3	8619.6-8620.6	8634.5-8640.4	Carquillat et al. (1997)
8662.0	Ca II	8651.0	8673.0	8634.5-8640.4	8684.4-8686.0	Solf (1978)
8679.4	Fe I	8676.9	8681.1	8634.5-8640.4	8684.4-8686.0	Ginestet et al. (1994)
8688.5	Fe I	8687.3	8690.6	8684.4-8686.0	8695.5-8698.0	Carquillat et al. (1997)
8710.2	Fe I	8708.5	8711.3	8704.2-8706.3	8714.5-8715.5	Kirkpatrick et al. (1991)
8712.8	Fe I	8711.3	8714.5	8704.2-8706.3	8714.5-8715.5	Kirkpatrick et al. (1991)
8747.4	Fe I?	8746.3	8748.4	8731.7-8733.8	8753.5-8755.6	Kupka et al. (2000)
8757.0	Fe I	8755.6	8758.8	8753.5-8755.6	8758.8-8761.0	Kirkpatrick et al. (1991)
8764.0	Fe I	8762.5	8765.0	8758.8-8761.0	8775.0-8777.0	Kirkpatrick et al. (1991)
8784.5	Fe I?	8783.4	8785.9	8775.0-8777.0	8786.0-8788.5	Kirkpatrick et al. (1991)
8793.2	Fe I	8791.5	8794.2	8786.0-8788.5	8810.0-8812.0	Kirkpatrick et al. (1991)
8805.0	Fe I	8803.3	8805.6	8786.0-8788.5	8810.0-8812.0	Kirkpatrick et al. (1991)
8824.0	Fe I	8823.2	8825.5	8810.0-8812.0	8828.5-8830.5	Kirkpatrick et al. (1991)
8838.0	Fe I	8837.5	8840.0	8828.5-8830.5	8850.0-8854.0	Kirkpatrick et al. (1991)

Table B.2 - Atomic lines measured. Taken from Dorda et al. (2016).

Molecular Band		
Bandhead centre (Å)	Chemical species	Reference
8432+8442+8452	TiO	Solf (1978)
8624.25	VO	Solf (1978)
8859.0	TiO	Valenti et al. (1998)

Table B.3 - Molecular bandheads measured. Taken from Dorda et al. (2016).